https://doi.org/10.5194/egusphere-2026-2524
Preprint. Discussion started: 28 May 2026

Inferring on-glacier meteorology from physical modeling and remote sensing

Shaoting Ren[1], Evan S. Miles[2,3,4], Michael McCarthy[1,2], Achille Jouberton[1], Thomas E. Shaw[1], Pascal Buri[6], Marin Kneib[2,5], Prateek Gantayat[1], Anneli Guthke[7] and Francesca Pellicciotti[1]

[1]Institute of Science and Technology Austria, ISTA, Klosterneuburg, Austria
[2]Swiss Federal Institute for Forest, Snow and Landscape Research (WSL), Birmensdorf & Sion, Switzerland
[3]Institute of Geography, University of Zurich, Zurich, Switzerland
[4]Department of Geosciences, University of Fribourg, Switzerland
[5]Institute of Environmental Engineering & Laboratory of Hydraulics, Hydrology and Glaciology, ETH Zurich, Zurich, Switzerland
[6]Geophysical Institute, University of Alaska Fairbanks, Fairbanks, USA
[7]Stuttgart Center for Simulation Science, University of Stuttgart, Stuttgart, Germany

Correspondence: Shaoting Ren (shaoting.ren@ist.ac.at)

Abstract. Local meteorology is crucial to understanding the response of mountain glaciers to climate change, yet it remains one of the largest sources of uncertainty in glacier modeling due to limited observations and complex glacier–atmosphere interactions. Recent advances in high-resolution, globally available remote sensing observations provide new opportunities to exploit observed glacier changes in order to infer high-mountain meteorology from climate reanalysis data. Here, we present a Bayesian framework combining physical energy and glacier mass balance modeling with remote sensing data to infer spatial bias corrections for on-glacier air temperature and precipitation. Our method performs a spatially-distributed inference using a physically-based land-surface model forced with statistically downscaled ERA5-Land reanalysis and an ensemble of bias-correction factors, with satellite-derived glacier surface albedo and surface mass balance as targets. The method is tested and evaluated at four benchmark glaciers in the European Alps and High Mountain Asia, with available independent in-situ observations. Results demonstrate that 1) Leveraging physical modeling with quantitative and multitemporal albedo observations can substantially reduce parameter equifinality in the inferred meteorological bias corrections; 2) Spatially-variable bias corrections improve the consistency between the model and the distributed satellite observations; 3) Compared to statistical downscaling, multi-year average air temperature and precipitation inferred with our framework show improved agreement with nearby station observations and more realistic spatial patterns over glaciers; 4) Our framework provides promising annual and seasonal mass balance with RMSEs relative to in-situ measurements of <1.5 m w.e. and <1 m w.e. respectively, corresponding to improvements of 40-50% and 20-60% compared to without inference. These results make this framework a promising avenue to derive spatial patterns of air temperature and precipitation as well as temporally-resolved glacier mass balance at the regional scale.

1 Introduction

Mountain glaciers are responding rapidly to a changing climate (Arndt and Schneider, 2023; Haeberli et al., 2007; Oerlemans et al., 1998). Knowledge of the meteorology and seasonal mass balance over glaciers is crucial to accurately understand this response, yet they remain challenging to quantify at the large scale (Aguayo et al., 2025; Barandun and Pohl, 2023; Marzeion et al., 2020). Mountain meteorological processes are complex and

https://doi.org/10.5194/egusphere-2026-2524
Preprint. Discussion started: 28 May 2026

include feedback mechanisms between the glacier surface and the atmosphere, making the spatio-temporal variability of the meteorological variables challenging to characterize and simulate (Immerzeel et al., 2014; Salerno et al., 2023; Shaw et al., 2021, 2024). These feedback mechanisms can include glacier cooling and elevation-dependent warming in high elevation areas (e.g. (Mackintosh et al., 2017; Pepin et al., 2022; Salerno et al., 2023), a strong influence of topography on precipitation patterns (e.g., Benoit et al., 2024; Immerzeel et al., 2014), and rapid changes in radiation balance through albedo evolution due to frequent transition in precipitation phase (e.g., Ding et al., 2014; Johnson and Rupper, 2020; Jouberton et al., 2022). In an ideal case, meteorological variables are directly measured using on- or nearby off-glacier Automatic Weather Stations (AWS), but such measurements are limited to a few individual glaciers over short time periods due to the relative inaccessibility of the sites and the difficulty of maintaining instruments in high mountain environments (Miao et al., 2024). Climate reanalysis products can provide global, long-term and high temporal resolution data in place of these meteorological observations, but they cannot be directly used to simulate glacier evolution given their coarse spatial resolution, inherent biases (Barandun and Pohl, 2023; Collier et al., 2024), simplicity of key physical processes on the glacier surfaces (Arduini et al., 2026) and the low density of high-altitude observations that are typically assimilated into them (e.g., Thornton et al., 2022). Large uncertainties in high mountain precipitation quantity and spatiotemporal variability make it challenging to estimate water resources for local and downstream hydrology and ecosystems (e.g., Aguayo et al., 2025; Graves et al., 2026; Ultee et al., 2026).

A common approach to derive reliable local meteorology within the cryospheric community involves downscaling climate reanalysis data and bias correcting them using available station observations (e.g., Fugger et al., 2022; Girona-Mata et al., 2024; Machguth et al., 2009; McCarthy et al., 2022; Shaw et al., 2022; Vogel et al., 2023). However, locally bias-correcting against station observations is infeasible for most glacier studies due to the scarcity of in-situ data on or near to glaciers. Moreover, the biases determined between station observations and climate reanalyses can be hard to extrapolate in space since sub-pixel processes, not well represented by the coarse reanalysis data, may or may not be detected by different in-situ data utilised (Buri et al., 2023; Cannon, 2018; Draeger et al., 2024; Immerzeel et al., 2014; Rye et al., 2010). For example, air temperature variability in mountain environments can be locally influenced by katabatic winds (Shaw et al., 2025), which in turn can be affected by the variable atmospheric and surface conditions (Sauter et al., 2026). Meanwhile precipitation can be significantly enhanced/reduced on windward/leeward slopes and be highly perturbed by the orientation of valley topography relative to the prevailing storm tracks. These challenges can create numerous modelling decisions when deciding how best to translate coarse reanalysis data into appropriate forcing data for glacio-hydrological modelling.

As an alternative to downscaling, past studies have inverted high-elevation meteorology from the outputs of glacio-hydrological models constrained with different types of data. Valéry et al. (2010) estimated precipitation vertical gradients in Sweden and Switzerland using observed runoff and simple water balance formulae. Oberrauch et al. (2024) leveraged in-situ snow depth data to correct spatiotemporal errors in air temperature, precipitation and incoming shortwave radiation over Switzerland. Glacier mass balance from remote sensing or in situ measurements is often used to bias-correct the air temperature and precipitation over glaciers or entire catchments. As the spatially integrated signal of glacier volume changes allows inference of precipitation

https://doi.org/10.5194/egusphere-2026-2524
Preprint. Discussion started: 28 May 2026

amounts, this approach has been used to bridge the spatial gap between point-based, station observations and large scale atmospheric models/reanalyses datasets. Immerzeel et al. (2015) corrected precipitation estimates in the upper Indus Basin by calibrating a degree-day model against glacier mass balance. Rounce et al. (2020) used a Bayesian approach to estimate temperature and precipitation biases using glacier-wide geodetic mass balance observations with a degree-day model (PyGEM - Python Glacier Evolution Model). Similar parameter inferences against globally-available geodetic mass balance observations are now commonly employed for large-scale glacier models (Rounce et al., 2023; Zekollari et al., 2024), but especially for simple temperature-index models, this single integrated target leads to equifinality. Model calibration against more refined spatial and temporal observations such as mass balance gradients or transient snowline altitudes has been suggested to be a key avenue to provide a representation of glacier processes and future evolution (Aberle et al., 2025; Cremona et al., 2025; Schuster et al., 2024). However, the lack of available stake mass balance still limits such a calibration to some specific glaciers, while the empirical degree-day melt models calibrated with snowlines or binary snow cover rely on simplified parameterizations that are not necessarily transferable in space or time due to poor representativeness of key physical processes such as surface radiation and heat fluxes, snow/ice sublimation (Bolibar et al., 2022).

Fully physical energy- and mass-balance models provide a more transferable approach for understanding glacier surface mass balance (Gabbi et al., 2014; Hock, 2005; Réveillet et al., 2018), but their more complex process representation also requires more observations to constrain them (Réveillet et al., 2018; Richter et al., 2026; Zolles et al., 2019). High-resolution, spatially distributed remote-sensing observations—such as altitudinally-resolved glacier surface mass balance with glacier elevation change and velocity (hereafter SMB - (Kneib et al., 2024; Miles et al., 2021), glacier surface albedo (Naegeli et al., 2017; Ren et al., 2021, 2024b; Williamson et al., 2025), or glacier surface temperature (Cook et al., 2014; Ren et al., 2024a)—are becoming increasingly available and provide opportunities for spatiotemporal and multi-objective constraints for model forcing, compared to single glacier-wide geodetic mass balance.

The aim of this study is to develop a generalized framework that derives a spatially distributed, bias-corrected meteorology over glaciers (namely air temperature and precipitation) and quantifies the associated uncertainty. Using Bayesian inference, the framework integrates a physical energy-balance model with multitemporal, spatially distributed remote sensing data of glacier albedo and altitudinally-resolved geodetic surface mass balance to ensure transferability and minimize parameter equifinality. We compare our approach against independent seasonal in situ mass balance data to evaluate the reliability of meteorological corrections and the potential of the approach to disaggregate multi-year mass balance. The method is developed and tested at four sites in distinct climatic regions, as well as over a larger catchment of the European Alps to evaluate its feasibility for large-scale applications.

2 Study sites

Study glaciers are selected based on the availability of stake measurements for glacier mass balance and meteorological observations. The sites are Argentière and Aletsch glaciers in the European Alps, Abramov Glacier in the northwest (Pamir) and Parlung No.4 Glacier in the southeast (Hengduan Mountain Range) of

https://doi.org/10.5194/egusphere-2026-2524
Preprint. Discussion started: 28 May 2026

High Mountain Asia (Fig. 1). The diversity of the sites allows us to evaluate our method in different climatic and glaciological conditions. Parlung No.4 Glacier has one on-glacier AWS which records air temperature, while the other glaciers have at least one off-glacier station in their vicinity (between 0.5 and 5 km from the glacier, Fig.1). Precipitation is measured with weighing gauge pluviometers and available in three of the sites: nine high-elevation stations surrounding Aletsch Glacier and Upper Valais, one station located at Chamonix ~8 km downstream of Argentière Glacier and one located ~6 km downstream of Parlung No. 4 Glacier, respectively. The European Alps belongs to the temperate climate zone with a winter accumulation regime and liquid precipitation falling in summer at the glacier terminus and their glaciers are characterized by a high mass turnover (Isotta et al., 2014); the Pamir region is continental and also characterized by winter accumulation and summer ablation, but with low mass turnover due to a drier (annual precipitation of ~1000 mm) and shorter ablation season compared to Europe, while the Hengduan Mountains are temperate but with a spring accumulation regime. Large elevation ranges (>1000 m) and complex topography enhance the spatial and temporal variability of the meteorology over these glaciers. In addition to these four sites, we use five clean ice glaciers in the Upper Valais region around Aletsch Glacier to test the feasibility of our method for larger areas (Fig. 1d).

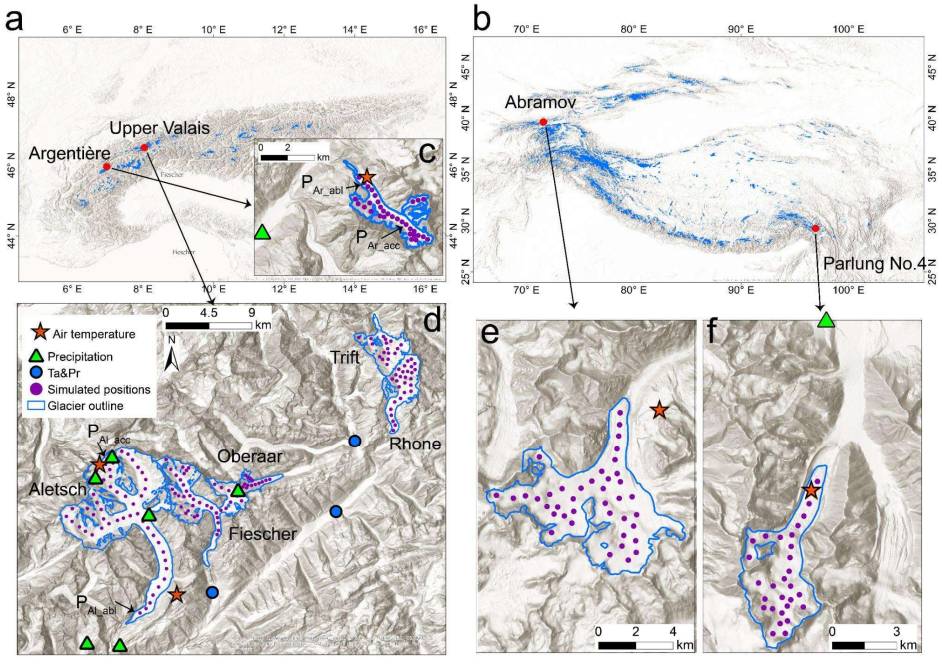

Figure 1. Study glaciers (c-f) and their location in the European Alps (a) and in High Mountain Asia (b). Stations measuring air temperature (Ta), precipitation (Pr) or both are represented by red pentagrams, green triangles and blue circles, respectively. Purple circles indicate the positions used for the Monte Carlo simulations (Section 3.4.3). Four stake mass balance measurements on Aletsch Glacier (P_{Al_abl} and P_{Al_acc} in Fig. 1d) and Argentière Glacier (P_{Ar_abl} and P_{Ar_acc} in Fig. 1c) are used to illustrate the details of the inference in Fig. 4 and Fig. S4, respectively. The glacier outlines are from the RGI 7.0 Consortium (2023). Background is the ESRI World Hillshade product (https://services.arcgisonline.com/arcgis/rest/services/Elevation/World_Hillshade/MapServer).

https://doi.org/10.5194/egusphere-2026-2524
Preprint. Discussion started: 28 May 2026

3 Methodology and datasets

We perform a distributed correction factor inference of air temperature and precipitation by coupling physical modeling with remote sensing observations using Bayesian inference (Richter et al., 2026). The primary objective is to identify simulations and correction factor sets of air temperature and precipitation that best reproduce satellite observations of distributed glacier surface albedo and surface mass balance. These observational datasets are selected as inference targets because of their strong links to key physical processes governing glacier melt and their sensitivity to meteorological forcing. The workflow consists of three main steps (Fig. 2): i) statistical downscaling of all ERA5-Land reanalysis data to force the energy-balance model (section 3.3), ii) a Bayesian inference methodology (section 3.4), including the definition of prior ranges for air temperature and precipitation correction factors, forward Monte Carlo simulations of the energy-balance model with those correction factors, and a likelihood weighting to obtain posterior correction factors, and iii) evaluation of the energy-balance model against independent datasets.

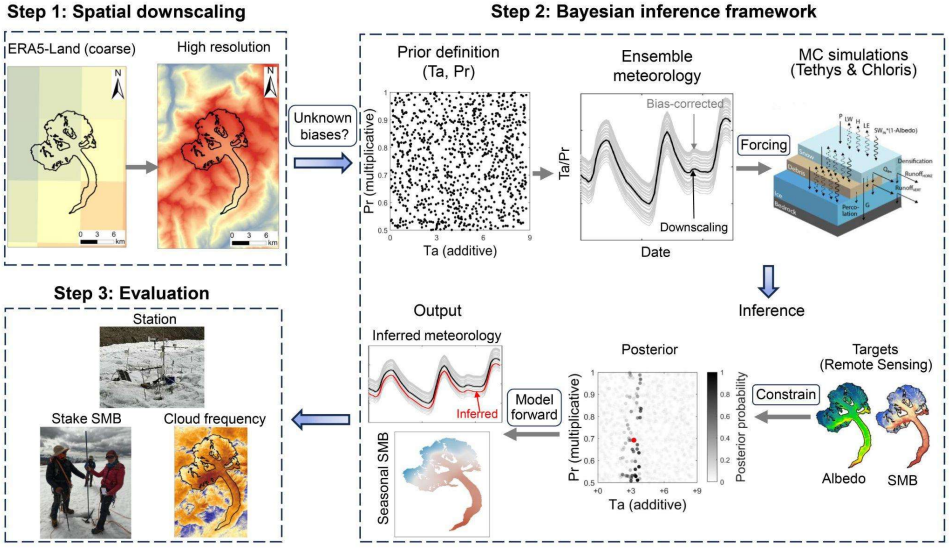

Figure 2. Flowchart of glacier meteorology inference. Step 1-3 are described in details in Section 3.3-3.5. Ta indicates air temperature, Pr indicates precipitation, MC indicates Monte Carlo, respectively.

3.1 Tethys & Chloris model

Glacier surface energy and mass balance is modelled using the fully physics-based land surface model Tethys & Chloris (hereafter 'T&C'; Fatichi et al. 2012a, b). T&C couples dynamics of energy, water and vegetation, and represents key physical processes for glacier surfaces, including surface radiation and heat fluxes, snow sublimation, snow compaction and refreezing (Fugger et al., 2022; Fyffe et al., 2021). The melt of glacier ice and snow is calculated by solving the surface energy budget. Precipitation is partitioned into rain, snow, and sleet phases following Ding et al. (2014) based on wet-bulb temperature. Snow albedo is calculated by taking into account fresh snowfalls, aging, sleet albedo, cloud cover, and sun angle (Ding et al., 2017), while ice albedo is constant in time and is defined by satellite observations (Section 3.2.1). The model also considers topographic

https://doi.org/10.5194/egusphere-2026-2524
Preprint. Discussion started: 28 May 2026

shading in the calculation of direct and diffuse radiation. It is run at 500 m spatial resolution and an hourly time step from 2014 to 2019, including one year model spin up. We do not calibrate maximum snow albedo (0.9), emissivity of snow and ice (0.97), maximum snow density in melting and frozen conditions (580 kg m^{-3} and 300 kg m^{-3}, respectively) and density threshold to transform snow into ice (500 kg m^{-3}), but baseline bare-ice and firn albedo are determined by the satellite-derived albedos to characterize the spatial variability of mean bare-ice albedo associated with surface properties (e.g., clean versus dirty or partially debris covered ice, and variations in roughness). These physical parameter sets have been demonstrated to be effective in a variety of settings (Buri et al., 2023; Fugger et al., 2024; Jouberton et al., 2025) and our goal is to develop a transferable, generally valid method to constrain equifinality between meteorological variables without tuning an optimal set of other parameters. As the modeling of debris-covered ice would introduce additional parameters such as debris thickness, thermal conductivity and aerodynamic roughness (e.g., Fontrodona-Bach et al., 2025; Melo-Velasco et al., 2025; Miles et al., 2022; Rounce et al., 2021) and our study glaciers are largely clean-ice, all glacier surfaces are set as ice. Debris cover accounts for 8-20% of total areas of Aletsch, Argentière and Abramov Glaciers and is present at the glacier termini. As such, our methodological configuration may introduce some uncertainties in inferred local meteorology, but only for the limited regions of the glacier terminus.

3.2 Target datasets

3.2.1 Glacier albedo

The first target for inference is glacier surface albedo from 2013 to 2022, which is retrieved using the algorithm of Ren et al. (2021) applied to Landsat-8 Collection 2 and Harmonized Sentinel-2 surface reflectance datasets. The algorithm explicitly accounts for anisotropic reflectance over snow and ice surfaces and shows good agreement with in-situ albedo measurements (Ren et al., 2021). Areas affected by cast shadows are identified by cast shadow modeling at the satellite overpass time, and are excluded from the analysis. Across the four study glaciers, there are >150 cloudless albedo scenes fairly distributed all year round at Aletsch and Abramov Glaciers, but only 92 scenes for Argentière Glacier due to mountain shadows during November-January and only 78 scenes for Parlung No.4 Glacier, all in winter to early spring due to monsoon during May-September (Fig. S1). All albedo datasets were aggregated to 100 m resolution to align T&C modeling. After removing snow albedo (>0.75), ice/firn albedo was determined as the lowest 10% percentile of remaining albedo values during the peak melt season (July and August). Ice albedos are considered spatially variable but temporally static in all modelling hereafter.

3.2.2 Surface mass balance (SMB)

The other main target for inference is an altitudinally-resolved surface mass balance dataset based upon Advanced Spaceborne Thermal Emission and Reflection Radiometer (ASTER) imagery (hereafter 'ASTER SMB'). This dataset provides a spatially distributed mass change and estimated by combining ASTER-based elevation changes from Hugonnet et al. (2021) with ice-flux divergence calculated from Landsat-8 and Sentinel-2 surface velocities and ice thickness from Millan et al. (2022), following the continuity approach (Cuffey and Paterson, 2010; Miles et al., 2021). ASTER SMB is derived for all four study glaciers, covering the period 2015-2019 at 100 m spatial resolution. Because this dataset relies exclusively on globally available products, it enables application of the method at regional to global scales. Evaluation against in-situ stake mass balance

https://doi.org/10.5194/egusphere-2026-2524
Preprint. Discussion started: 28 May 2026

(hereafter 'stake SMB') shows that uncertainty of ASTER SMB varies significantly across the four glaciers, with underestimation of mass loss in the ablation regions of Parlung No.4 Glacier (2-6 m w.e. a^{-1}) and Argentière Glacier (~2 m w.e. a^{-1}), while other glaciers generally show a good accuracy (Fig. S2).

To explore the sensitivity of the inferred glacier meteorology (Section 3.4) to the quality of SMB information, two alternative approaches are considered. The first is to run our inference approach with the stake SMB as the target (at the stake measurement locations), to assess the consistency between a ground "truth" and the ASTER SMB. The second is to compare the inference results between the ASTER SMB and higher resolution geodetic information available at two of the glaciers. The first high resolution SMB dataset is derived from 2 m Pléiades digital elevation models and velocity fields over the period 2012–2022 on Argentière Glacier (hereafter Pléiades SMB), constrained by in situ ice thickness measurements and processed using the average of three independent approaches to derive SMB (Kneib et al., 2024). For Aletsch Glacier, a TanDEM-X elevation change and surface velocities dataset is obtained using interferometric synthetic aperture radar (InSAR) over the period 2011–2017 (hereafter TanDEM-X SMB - Leinss and Bernhard, 2021). As for albedo, all these three datasets are aggregated to 100 m resolution.

3.3 Spatial downscaling of ERA5-Land for climatic inputs

We use seven meteorological variables from hourly ERA5-Land reanalysis data as forcing data for T&C, namely: air temperature (Ta), total precipitation (Pr), incoming shortwave radiation, incoming longwave radiation, relative humidity, air pressure, and wind speed. Compared with other reanalysis products, such as ERA5, MERRA-2, and JRA-55, ERA5-Land provides a higher spatial resolution (~9 km; Muñoz-Sabater et al., 2021) and a better-resolved glacier/snow surface component. Following Machguth et al. (2009) and McCarthy et al. (2022, 2025), these variables are statistically downscaled to a set of locations across the glaciers where we run the T&C model (purple dots in Fig. 1). Air temperature and dewpoint temperature are downscaled to the surface elevation of the respective location using monthly-hourly average lapse rates calculated from pressure levels of ERA5 centered over the point of interest. Precipitation is downscaled with a simple spline interpolation. A static elevation gradient derived from 5*5 neighboring grids of ERA5-Land (0.719 mm yr^{-1} m^{-1}) is applied at Aletsch Glacier, whereas no precipitation lapse rate is used for the other glaciers due to the absence of a clear altitudinal gradient. Incoming shortwave radiation is downscaled using a thin-plate spline interpolation, as topographic corrections are applied internally within T&C. Relative humidity is derived from the downscaled air and dewpoint temperatures, following Rouf et al. (2020). Atmospheric pressure and incoming longwave radiation are downscaled following Cosgrove et al. (2003), while wind speed is downscaled using the method of Liston and Elder (2006). The ERA5-Land domains are centered over the glacier of interest considering at least one pixel buffer around any pixels intersecting the glacier area. Downscaled multi-year average air temperature and precipitation can be seen in Fig. S3. These spatially downscaled datasets serve as the initial meteorological forcing and are used to generate ensemble inputs for the Monte Carlo simulations (Section 3.4.2).

3.4 Bayesian inference framework

To determine the set of air temperature and precipitation correction factors and their uncertainties, we need to identify the simulations that match satellite observations well. Bayesian inference is a useful framework for this

https://doi.org/10.5194/egusphere-2026-2524
Preprint. Discussion started: 28 May 2026

purpose, and has been used to determine the most plausible parameters of degree-day melt model and their uncertainties in the cryospheric community (e.g., Khadka et al., 2024; Rounce et al., 2020; Verjans et al., 2020). The approach combines prior knowledge about the inferred parameters of interest (θ) with the evidence in observed data (y) to obtain a posterior probability distribution $p(\theta|y)$ that represents the posterior state of knowledge about θ after taking into account the information in the observed data:

$$p(\theta|y) = \frac{p(\theta)p(y|\theta)}{p(y)} \quad (1)$$

where $p(\theta)$ is the prior distribution of θ, which reflects expert knowledge and is here assumed to be a uniform distribution (see Section 3.4.1 for more details) and hence a constant within its bounds; $p(y|\theta)$ is the probability of the data given the model's predictive distribution for a given θ (likelihood); $p(y)$ is the marginal distribution of the data and can be regarded as a normalization constant. Therefore, Eq. 1 can be rewritten as:

$$p(\theta|y) \propto p(y|\theta) \quad (2)$$

In this study, θ corresponds to the correction factors of temperature and precipitation. Correction factors for air temperature are additive, whilst precipitation factors are multiplicative. To establish a likelihood function, we assume a normal distribution of errors, expressed as the distance of multitemporal albedos and one multi-year average SMB between the model simulations and remote sensing observations (Rounce et al., 2020). The joint likelihood function can be expressed as a multiplication of both albedo ($p(y_{alb}|\theta)$) and SMB ($p(y_{smb}|\theta)$) terms:

$$p(y|\theta) = p(y_{alb}|\theta) * p(y_{smb}|\theta) \quad (3)$$

with

$$p(y_{alb}|\theta) = \frac{1}{\sqrt{2\pi\sigma^2_{alb}}}\, exp[-\sum_1^{N_{alb}}(\hat{y}_{alb} - \bar{y}_{alb})^2/2\sigma^2{}_{alb}] \quad (4)$$

$$p(y_{smb}|\theta) = \frac{1}{\sqrt{2\pi\sigma^2_{smb}}}\, exp[-\sum_1^{N_{smb}}(\hat{y}_{smb} - \bar{y}_{smb})^2/2\sigma^2{}_{smb}] \quad (5)$$

where $\hat{y}_{alb}$ and $\hat{y}_{smb}$ are modelled albedo and SMB, $\bar{y}_{alb}$ and $\bar{y}_{smb}$ are remotely sensed albedo and SMB, and N_{alb} and N_{smb} are the number of available remote sensing observations, in our case N_{alb} varies depending on available albedo scenes and N_{smb}= 1 for all glaciers. The deviations between simulated and observed values are assumed to be Gaussian distributed with standard deviations σ_{alb} and σ_{smb}. We consider both observation uncertainty (σ_{alb_s} and σ_{smb_s}) and model errors ($\sigma_{alb_m}$and σ_{smb_m}):

$$\sigma^2{}_{alb} = \sigma^2{}_{alb\_s} + \sigma^2{}_{alb\_m} \text{ and } \sigma^2{}_{smb} = \sigma^2{}_{smb\_s} + \sigma^2{}_{smb\_m} \quad (6)$$

where σ_{smb_s} is derived from processing of the geodetic SMB at pixel scale (e.g., Miles et al., 2021), and σ_{alb_s} is set to 0.07 from comparison between satellite and in-situ albedos on the six glaciers (RMSE = 0.07, Ren et al., 2021). The standard deviation of model errors σ_{alb_m} is set to 0.2, which corresponds to the RMSE of T&C outputs against satellite albedo observations (Buri et al., 2023) and $\sigma_{smb_m}$is set to 0.2 m w.e., based upon the validation of T&C outputs against stake mass balance measurements for several mountain glaciers (Fugger et al., 2022; Fyffe et al., 2021).

Since a Markov Chain Monte Carlo implementation as in, e.g. Rounce et al. (2020), is computationally unfeasible for our study with a full energy balance model, we approximate the Bayesian posterior solution with a "low-budget brute-force" Monte Carlo approach, given 1000 total realizations per location on the glacier (N_{MC}). We draw a limited number N_{MC} of realizations (see Section 3.4.3) from the prior distribution (see Section 3.4.1) and assess the plausibility of each Monte Carlo simulation by evaluating its likelihood. The posterior

https://doi.org/10.5194/egusphere-2026-2524
Preprint. Discussion started: 28 May 2026

mean of the inferred bias-correction values of air temperature and precipitation ($\theta_{inferred}$, red point in Fig. 4 and Fig. S4) can be approximated via simple Monte Carlo integration (Hammersley, 1960) by:

$$\theta_{inferred} = \sum_{i=1}^{N_{MC}} \theta_i * \frac{p(y|\theta_i)}{\sum_{i=1}^{N_{MC}} p(y|\theta_i)} \quad (7)$$

and the corresponding posterior bias-correction uncertainty can be characterized by Bayesian credible intervals. Here, we consider the 90 % credible interval, i.e., we wish to extract the interval bounds of the posterior distribution where 90 % of the probability mass accumulates, approximated by the 5th and 95th quantile of the weighted Monte Carlo sample. To monitor the statistical reliability of our small ensemble size, we determine the effective sample size (ESS), i.e., the number of realizations that effectively contributed to posterior statistics, as calculated by (Liu, 2004):

$$ESS = 1/(\frac{p(y|\theta_i)}{\sum_{i=1}^{N_{MC}} p(y|\theta_i)})^2 \quad (8)$$

Large ESS values indicate that the constraining effect of the target data is small, i.e., equifinality exists in the given configuration. Very small ESS values, on the other hand, reveal that only very few correction factor values are able to fit the data sufficiently well. While very small ESS values would spoil a reliable statistical analysis (e.g., investigating the shape of the posterior distribution in further detail, which is beyond the scope of this study), they identify scenarios of high identifiability and are hence of interest to us. Therefore, even with a limited computational budget, we can draw valuable insights from this inference framework and shed light on distinct spatial patterns of bias corrections, and the potential of physical modeling with multitemporal observations to reduce equifinality.

3.4.1 Establishing priors

Previous studies have highlighted the critical importance of the initial parameter ranges (i.e., priors in Bayesian inference; Sjursen et al., 2023). Here we leverage two sources of prior knowledge: 1) For air temperature, a global evaluation over monitored glaciers reports that downscaled ERA5-Land shows a warm bias of +1.41 °C during summer, with most biases falling within the range of −2 to +5 °C (Shaw et al., 2025), which thus would result in an additive factor for air temperature ΔTa in the interval [-5, +2]; 2) For precipitation, we assume a range of biases from -50% to +200% (e.g., Khadka et al., 2022; Torre et al., 2024; Wu et al., 2023), resulting in a multiplicative precipitation factor k_p range of [0.5, 3]. Since we are running a fully physically based energy and mass balance model, such wide ranges result in too high computational costs. Therefore, we explicitly incorporate prior knowledge of biases in the glacier meteorological forcing to establish narrow priors (Cremona et al., 2025), Fig. 3). This pre-inference step is performed for each simulated location (purple dots in Fig. 1c-f and Section 3.4.3) to account for spatial variability of ERA5-Land biases, i.e. a location-specific prior. The main idea is determining the priors by physically interpreting the discrepancy between modelled SMB (Mod_{SMB}) and satellite observation (Sat_{SMB}): when Mod_{SMB} is more positive than Sat_{SMB}, air temperature should be higher and/or precipitation should be lower, and we therefore fix k_p as [0.5, 1] since we have known that the low boundary is 0.5, and determine low boundary of ΔTa using k_p= 0.5 and upper boundary of ΔTa using k_p= 1; otherwise, we fix ΔTa as [-5, +2] and determine the range of k_p. This pre-screening step is computationally much less demanding than the Monte Carlo simulations we use on the inference (see Section 3.4.3). Compared to Pléiades and stake SMB, k_p determined by ASTER SMB is higher at Argentière and Parlung No.4 Glaciers

https://doi.org/10.5194/egusphere-2026-2524
Preprint. Discussion started: 28 May 2026

due to underestimation in mass loss (Fig. S4) and its impact is discussed in Section 5.2.

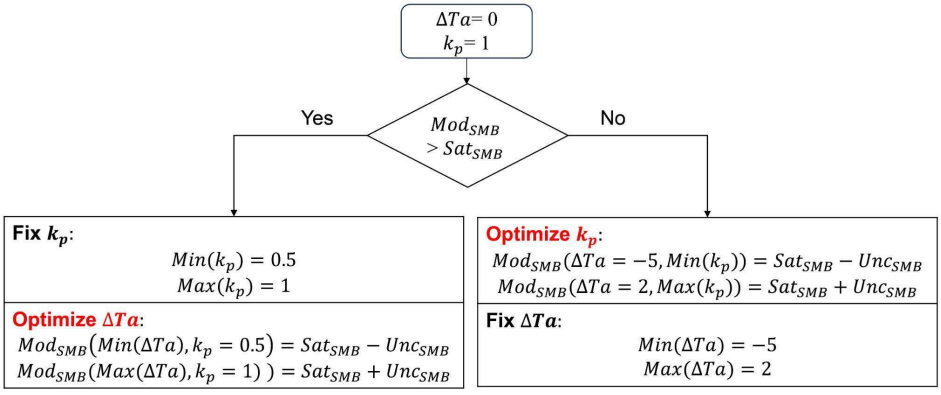

Figure 3. Flowchart of prior definition for each simulated position (purple points in Fig. 1c-f). ΔTa is the additive factor for air temperature (Eq. 9), k_p is the multiplicative factor for precipitation (Eq. 15), Mod_{SMB} is modelled SMB, Sat_{SMB} is satellite SMB and Unc_{SMB} is the uncertainty of satellite SMB, respectively.

3.4.2 Ensemble of forcing data

An ensemble of forcing datasets is generated by randomly sampling N_{MC} correction factors for air temperature precipitation from uniform distributions within the defined prior ranges. An additive factor (ΔTa [°C]) is applied directly to the downscaled ERA5-Land time series:

$$Ta_{Adj} = Ta + \Delta Ta \quad (9)$$

where Ta_{Adj} [°C] is adjusted air temperature and Ta [°C] is downscaled air temperature. To ensure physical consistency, dew point air temperature ($Tdew_{Adj}$) is adjusted based on modified vapor pressure e_{Adj} [Pa] and saturation vapor pressure $esat_{Adj}$ [Pa] using Ta_{Adj} (Shuttleworth. 2012) and keeping the relative humidity RH [-] constant:

$$Tdew_{Adj} = -\frac{273.3}{1-17.27/ln\,(e_{Adj}/611)} \quad (10)$$

$$e_{Adj} = RH * esat_{Adj} \quad (11)$$

$$esat_{Adj} = 611 * exp\,(\frac{17.27*Ta_{Adj}}{Ta_{Adj}+273.15}) . \quad (12)$$

Incoming longwave radiation ($LW\downarrow_{Adj}$ [W m^{-2}]) is adjusted by adding longwave radiation caused by changing air temperature based on Stefan Boltzman law and unchanged air emissivity (ε [-]):

$$LW\downarrow_{Ta,Adj} = \varepsilon * \sigma * (Ta_{Adj} + 273.15)^4 \quad (13)$$

$$\varepsilon = \frac{LW\downarrow}{\sigma*(Ta+273.15)^4} \quad (14)$$

where $LW\downarrow$ [W m^{-2}] is downscaled longwave radiation, $LW\downarrow_{Ta}$[W m^{-2}] and $LW\downarrow_{Ta,Adj}$ [W m^{-2}] are the longwave radiation terms estimated from the downscaled and bias-corrected air temperature, respectively, and σ is the Stefan Boltzmann constant (5.67e^{-8} W m^{-2} K^{-4}). For precipitation, a multiplicative factor (k_p) is applied to preserve the timing and frequency of precipitation events:

$$Pr_{Adj} = Pr * k_p \quad (15)$$

https://doi.org/10.5194/egusphere-2026-2524
Preprint. Discussion started: 28 May 2026

where Pr_{Adj} [mm] is corrected precipitation and Pr [mm] is downscaled precipitation. We apply seasonally varying precipitation corrections, with correction factors for the four meteorological seasons (JFM, AMJ, JAS, OND), as previous studies have documented pronounced seasonal biases in ERA5-Land precipitation in regions such as High Mountain Asia (Jouberton et al., 2025). No seasonal correction is applied to air temperature, both to limit the dimensionality of the inference problem and to avoid temporal jumps of the continuous temperature time series across seasons.

3.4.3 Simulation-inference framework

To balance computational efficiency and spatial representativeness, we develop a two-step simulation–inference framework. Firstly, simulations are performed at locations around the central flowline of each glacier at ~500 m spacing (purple dots in Fig. 1c-f), with N_{MC}=1,000 Monte Carlo simulations at each location (hereafter simulated location). Secondly, to obtain more distributed sampling without new simulations, inference is conducted on a regular 100 m × 100 m grid (hereafter inferred location, crosses in Fig. 7e-h) by assigning the Monte Carlo ensemble of the nearest three-dimension distance to a simulated location. For Aletsch Glacier, ~3,000 inferred locations are randomly selected to reduce computation cost (Fig. 7f), evenly distributed across elevation bands to ensure adequate spatial representativeness. This framework assumes that grid cells within a 500 m × 500 m neighborhood share the same Monte Carlo ensemble, which is reasonable given their similar model inputs and parameter configurations. Spatial variability in air temperature and precipitation within a 500 × 500 m grid is deemed small enough to be determined by a single Monte Carlo simulation. Inferred locations at glacier margins are excluded using a 150 m buffer to avoid areas with high uncertainty in surface mass balance and strong topographic shading, where fewer valid satellite albedo observations are available. Finally, the inferred meteorology (the downscaled meteorology with the posterior mean biases applied) and their associated uncertainties (5th and 95th quantile of posterior distribution) are spatially interpolated across the entire glacier using spline interpolation.

To obtain spatially distributed seasonal SMB, the inferred bias-correction parameters ($\theta_{inferred}$) are applied to the meteorological forcing at each inferred location, and the T&C model is rerun using the corrected inputs.

3.4 Evaluation of inferred meteorology

Three complementary steps are used to evaluate the inferred glacier meteorology. 1) We evaluate inferred air temperature against AWS observations and precipitation with weighing gauge pluviometers records (hereafter 'station observations' for clarity, Fig. 1c-f), including one on-glacier air temperature observation at Parlung No.4 Glacier. All the evaluations for precipitation are conducted between station observations and the nearest locations on the glacier, to provide an indication of how well the inferred meteorological fields align with available station observations. 2) Spatial patterns of catchment total precipitation are qualitatively evaluated by comparing against the cloud frequency derived from satellite imagery, calculated over glacier surfaces using the Sentinel-2 cloud "probability" band (range 0–1; Zupanc, 2017). Pixels are classified as cloudy when the cloud probability exceeds 0.5, and mean cloud frequency is computed for the period 2015–2019. 3) We also use the modelled seasonal surface mass balance obtained with the forward model to indirectly evaluate the inferred meteorology and test the method's ability to represent the seasonality of mass balance when constrained

https://doi.org/10.5194/egusphere-2026-2524
Preprint. Discussion started: 28 May 2026

against only a single snapshot of mass balance from the ASTER SMB estimate. All independent stake SMB data are used to make this evaluation using the RMSE as the metric (Table S1).

4 Results

4.1 Performance of the inference

Posterior distributions of the Bayesian inference demonstrate that quantitative and multitemporal target datasets can largely reduce the equifinality of temperature bias and precipitation factor derivation from the glacier energy balance model. As an example, the posterior distributions of ΔTa and k_p at four stake positions of Aletsch and Argentière Glaciers show a much narrower parameter space when using multitemporal albedo observations or stake SMB compared with the use of a single ASTER or TanDEM-X SMB target (Fig. 4 and S5), corresponding to a very small effective sample size of multitemporal targets (4 to 50) compared to >300 for single SMB datasets. The narrow space inferred with satellite albedo and ASTER/TanDEM-X SMB is closer to using albedo-only than SMB-only, indicating that the inference fuses the information of both targets through compensations between them, but is dominated by satellite albedo due to its narrow parameter space.

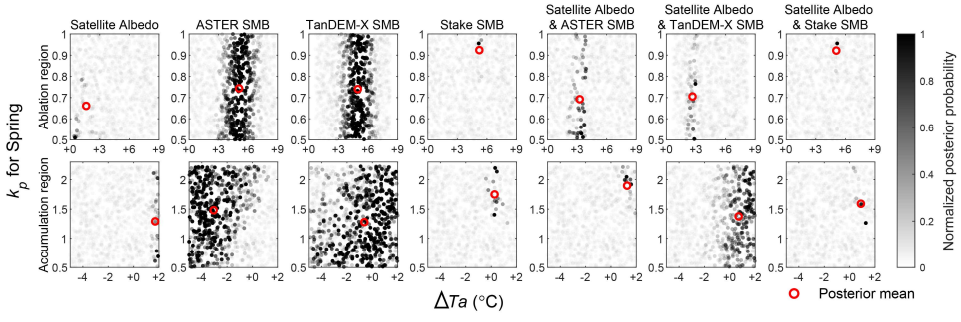

Figure 4. Two examples of Monte Carlo posterior samples (intensity-coded by their normalized posterior probability) distributions and inferred (posterior mean) bias-correctors for seven different combinations of targets at two stake SMB measurements at the ablation and accumulation region of Aletsch Glacier (marked P_{Al_abl} and P_{Al_acc} in Fig. 1d). Black points are 1000 Monte Carlo simulations. Note that the period of ASTER SMB is 2015-2019, while TanDEM-X SMB is 2011-2017. See Fig. S5 for other examples at Argentière Glacier.

The results show that modelled albedo and SMB have substantially improved agreement with the target datasets for most glaciers, compared to simulations driven by downscaled meteorology without optimisation of ΔTa and k_p. Compared with downscaling alone, the modelled SMBs are closer to the 1:1 line with RMSEs generally reduced by 0.3-2 m w.e., and the RMSEs of modelled albedos reduced by 0.02-0.06 (Fig. 5 and S7). Similar spatial patterns of modelled SMB compared to satellite observations (Fig. 6 and S8), smaller RMSEs for albedo in most elevation bands and better modelled temporal variability of albedo (Fig. S9) further indicate an improved performance with our inference. The largest improvement is for the Abramov Glacier (Fig. S7b), for reasons we discuss later (Section 5.3). Improvements in modelled SMBs are greater when inferred against stake measurements than when inferred against satellite observations (cf. Fig. 5a with Fig. 5b+c), indicating the importance of accurate and multitemporal observations. This is exemplified for Argentière Glacier in Fig. 5, a

https://doi.org/10.5194/egusphere-2026-2524
Preprint. Discussion started: 28 May 2026

site with a large availability of stake data and high resolution Pléiades SMB. The results for other glaciers are shown in Fig. S7.

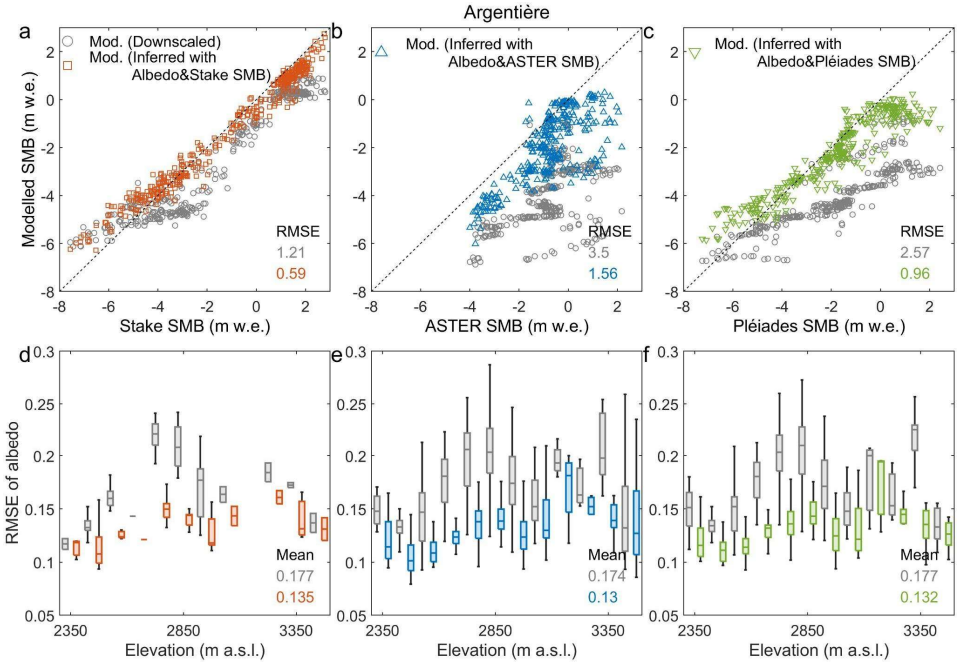

Figure 5. modelled SMB (a-c) and glacier albedo (d-f) against targets at Argentière Glacier (see Fig. S5 for other glaciers). Grey dots/bars represent the modelled mass balances/albedos with only downscalling of ERA5-Land (without bias-correction), orange dots/bars are those inferred with satellite albedo and stake SMB, blue is inferred with satellite albedo and ASTER SMB, and green is inferred with satellite albedo and Pléiades SMB. Note that the points in panel a) represent all measurements from 78 stakes, while in panel b) and c) they represent all locations where inference was conducted (see black dots in Fig. 7e).

4.2 Inferred meteorology at individual and catchment scales

With satellite albedo and stake/ASTER SMB as targets, the inferred bias-correction factors strongly vary spatially across each glacier, especially for precipitation correction factors, which range from 0.7 to >2.5 (Fig. S10-11), leading to more spatially and elevationally variable complex patterns of inferred multi-year meteorology compared to the downscaling alone (Fig. 6 and 7+S3). The inferred air temperatures remain elevation-dependent, but the equivalent lapse rates are typically shallower (except for Abramov Glacier) and less linear compared to the downscaled air temperatures. Inferred precipitation also exhibits altitudinal patterns, with strong local variations at all glaciers compared to statistically downscaled precipitation (Fig. 6). We observe a general consistency between cloud frequency (Fig. S12) and precipitation (Fig. 7m-p) which suggests that the spatial pattern of precipitation obtained through the inference is robust. Moreover, evaluation at Aletsch Glacier, the only study site with multi-station precipitation observations, shows that both inferred and station observed precipitation exhibit positive vertical patterns and gradually increase from 1100 mm at the terminus to >4000 mm at the top (Fig. 6b and 7n).

https://doi.org/10.5194/egusphere-2026-2524
Preprint. Discussion started: 28 May 2026

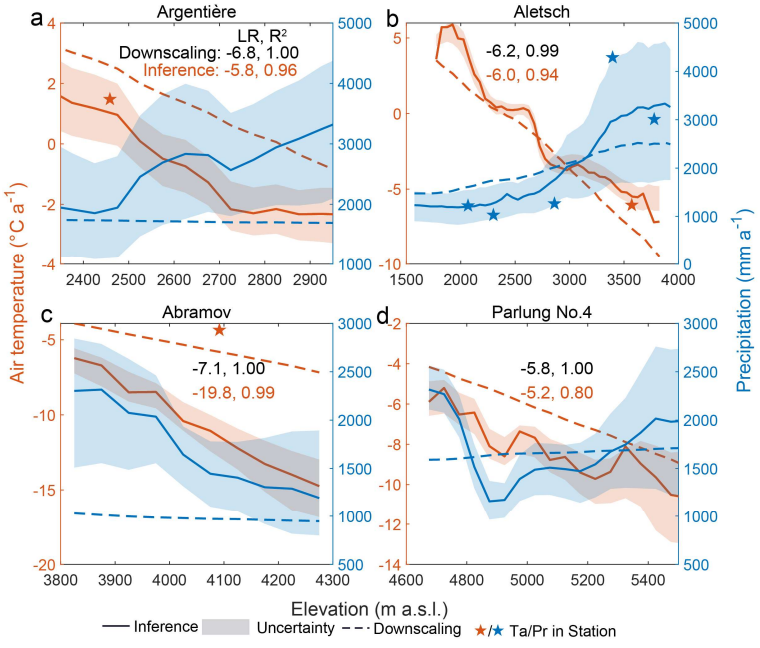

Figure 6. Downscaled and inferred multi-year average air temperature and precipitation by satellite albedo and ASTER SMB datasets as a function of elevation at the four tested glaciers during 2015-2019. The red/blue pentagrams indicate air temperature (Ta)/precipitation (Pr) of the station observations. Black numbers indicate lapse rate of air temperature (LR, °C km^{-1}) and R^2 for downscaled ERA5-Land, while red numbers are for inferred air temperature. The shaded area represents the uncertainty of inferred meteorological variables in each elevation bin. The dataset used for aggregation is the same as in Fig. 7 and S3.

https://doi.org/10.5194/egusphere-2026-2524
Preprint. Discussion started: 28 May 2026

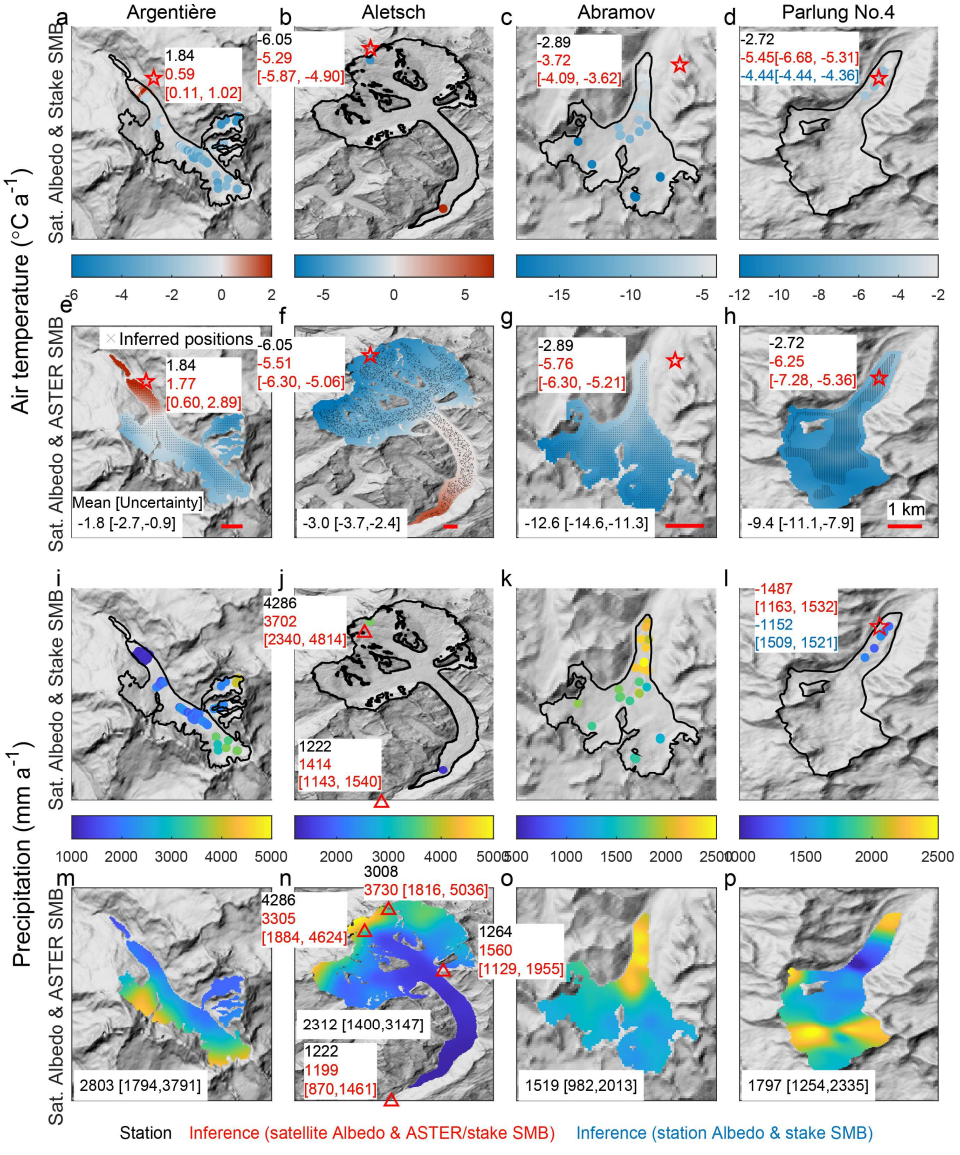

Figure 7. Inferred multi-year average air temperature (a-h) and precipitation (i-p) using stake SMB (a-d and i-l)/ASTER SMB (e-h and m-p) and multitemporal albedo as targets across four glaciers during 2015-2019. Points are the positions of stake SMB and their colors represent inferred meteorology, crosses in panel e-h are the positions used for inference with two satellite targets (Section 3.4.3). The locations of station observations are marked with red pentagrams (air temperature) and triangles (precipitation), with the black numbers representing the station observations, red and blue numbers representing inferences and associated uncertainties with different targets. The numbers in the left corner represent the glacier-wide mean and associated uncertainty. Note that the color bar for each glacier is the same for clear comparison between different targets.

Air temperature and precipitation inferred using both stake and ASTER SMB are similar for most glaciers

https://doi.org/10.5194/egusphere-2026-2524
Preprint. Discussion started: 28 May 2026

except the ablation region of Parlung No.4 Glacier (Fig. 7l and 7p) where satellite-derived mass loss is strongly underestimated by 3-6 m w.e. a^{-1} (Fig. S2). For the terminus of Parlung No.4 Glacier, precipitation is distinctly overestimated using the ASTER SMB target, compared to the stake SMB target, showing a local maximum >2000 mm (red rectangle in Fig. 7p). The precipitation inferred with stake SMB at the ablation region of Parlung No.4 is about 1400 mm (Fig. 7l), which is closer to the 500 mm recorded ~5 km downstream of the glacier terminus. Moreover, we also notice that inferences with stake or ASTER SMB targets show a surprisingly inverse precipitation gradient for Abramov Glacier (purple rectangles in Fig. 7k and 7o), that is inconsistent with the cloud frequency pattern (Fig. S12c). Again, we discuss potential causes and implications of this in Section 5.3.

When exploring the inferred meteorology over the broader Upper Valais domain, we observe consistent annual magnitudes across the five neighboring glaciers (Fig. 8a-b and Fig. S13). For example, in the Aletsch, Fiescher and Rhone valleys, annual precipitation rises from ~1000-1200 mm at downstream stations (4-13 km to glacier termini) to 1200-1600 mm at glacier termini themselves (Fig. 8b). Precipitation reaches >3000 mm along the upper mountain crests of neighboring Aletsch and Fiescher glaciers and neighboring Trift and Rhone glaciers. Positive correspondence between precipitation and cloud frequency are observed over Aletsch and Fiescher glaciers (Fig. 8d), where precipitation increases sharply from ~2000 mm to >4500 mm in the upper extents, and cloud frequency correspondingly increases from 40% to 60% (Fig. 8b-d). This is reasonable since clouds can be blocked along windward slopes and accumulate near mountain crests, therefore leading to a similar spatial pattern observed for the inferred precipitation.

https://doi.org/10.5194/egusphere-2026-2524
Preprint. Discussion started: 28 May 2026

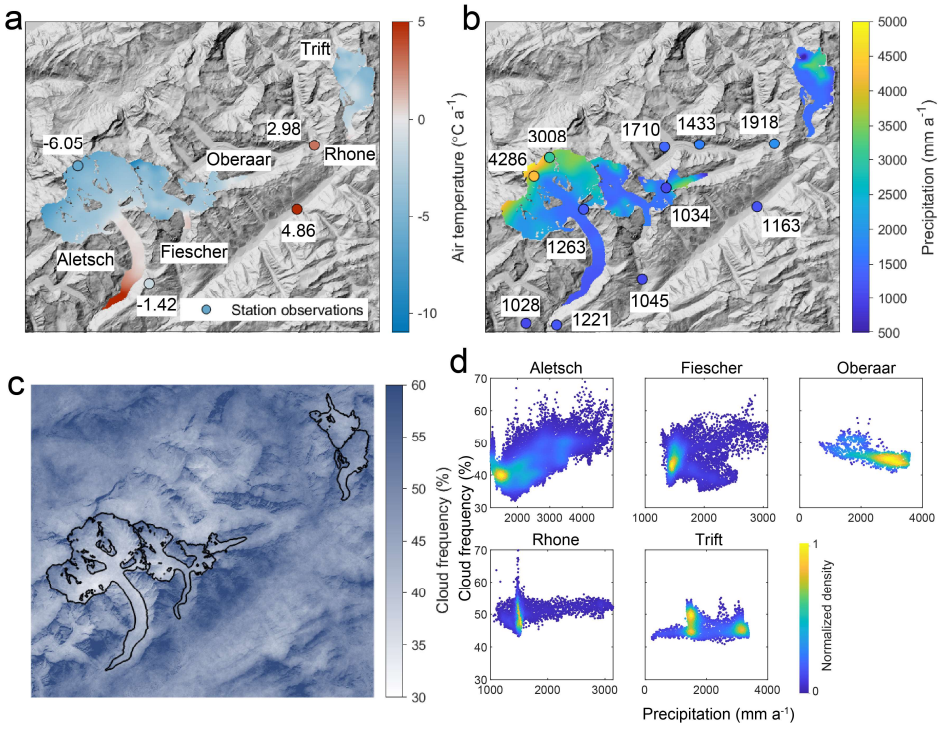

Figure 8. Multi-year average of air temperature (a) and precipitation (b) inferred with ASTER SMB and compared to station observations and cloud frequency (c-d) across multiple glaciers in the Upper Valais of the central Alps during 2015-2019. The locations of station observations are marked with circles; the colors and the black numbers indicate their annual values. The names of five glaciers are indicated in panel (a). Data used in panel (d) are derived from on-glacier pixels in panels (b) and (c), the y-axes are consistent across all subpanels, while the x-axes differ for clarity.

4.3 Inferred annual/seasonal mass balance

Compared with simulations forced by statistical downscaling alone, modelled mass balances constrained with albedo and ASTER SMB show substantially improved agreement with stake measurements, both annually and seasonally (Fig. 9). RMSE values are reduced to <1.5 m w.e. for annual mass balance with improvements of 20-60%, and <1 m w.e. for seasonal mass balance with 40-50% improvement across most glaciers. The distribution of data points generally lies along the 1:1 line for both negative and positive mass balances (Fig. 9), further highlighting the value of the remotely sensed information to infer spatially variable temperature and precipitation corrections over the glaciers, complementing the limited evaluation possible with station data alone. Only Parlung No.4 Glacier shows a worse SMB after inference due to the clear underestimation of mass loss in the ASTER SMB target compared to local stake data (Fig. S2), highlighting the value of high quality distributed SMB data for this approach. Furthermore, slight underestimations for large mass loss at most glacier termini also indicate other limitations of the methodology, such as replacement of debris as clean ice in the model (Section 3.1). Nevertheless, the general improvements of mass balance against independent observations not only confirm the capability of the method to meaningfully adjust on-glacier meteorology (cf. Fig. 7-8), but

https://doi.org/10.5194/egusphere-2026-2524
Preprint. Discussion started: 28 May 2026

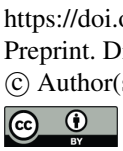

also indicate a promising way to leverage widely available satellite SMB datasets for a single snapshot with multi-temporal albedo data to reproduce the seasonality of mass changes over distinct regions.

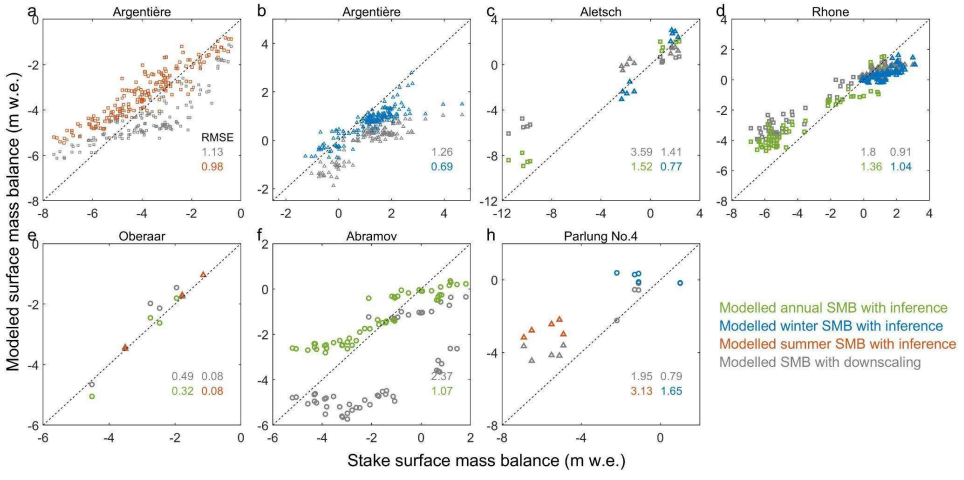

Figure 9. Annual/seasonal mass balance forced by downscaled and inferred meteorology against in-situ stake surface mass balance on the six studied glaciers. Each point represents an individual stake mass balance measurement.

5 Discussion

5.1 Importance of quantitative and multitemporal satellite albedo

Posterior distributions of air temperature and precipitation correction factors inferred with satellite albedo only show that meteorological parameter equifinality can be largely reduced compared to the inference with satellite SMB only (Fig. 4 and S5). Compared with only one multiyear average value, satellite-derived albedo data can provide valuable temporal information regarding the expected balance of air temperature, precipitation and the related glacier energy balance, thus providing a more constrained parameter space. Similarly, recent studies have shown the key value of temporal satellite snow cover data for the improvement of empirical degree-day glacier modeling (Aberle et al., 2025; Cremona et al., 2025). However, unlike binary snow cover data (i.e. snow-covered or not), quantitative satellite albedo can provide more information of glacier surface evolution, including fresh snow, granular snow, firn, pure ice and dirty ice, thus further narrowing the posterior distribution. Since stake SMB are only available for limited glaciers, this finding shows that leveraging more quantitative and multitemporal satellite targets such as albedo is promising to solve model over-parameterization. Similarly, two recent local-scale studies for an Arctic glacier (Cao et al., 2025) and for a mountain glacier (Richter et al., 2026) have highlighted the value of satellite albedo in improving glacier energy-balance modeling.

5.2 Impact of SMB accuracy

The observed ASTER SMB helps us define the prior range of air temperature and precipitation corrections (Section 3.4.1) and serves as an inference target. ASTER SMB uncertainty can be larger and more varied in space than satellite albedo due to the variable way in which it is calculated (Section 3.2.2), including small

https://doi.org/10.5194/egusphere-2026-2524
Preprint. Discussion started: 28 May 2026

errors for Aletsch Glacier (<1 m w.e. a^{-1}), moderate underestimation for Argentière Glacier (~2 m w.e. a^{-1}) and large underestimation for Parlung No.4 Glacier (3-6 m w.e. a^{-1}, Fig. S2). These underestimations of mass balance by the ASTER data can lead to inappropriate prior ranges at the terminus of glaciers, including a wider precipitation prior of [0.5, 2] for Argentière Glacier compared to the Pléiades SMB (Fig. S4a-b), or a more restricted and colder air temperature prior range and a much more positive precipitation prior for Parlung No.4 Glacier, compared to stake SMB (Fig. S4e-f). As a consequence, the annual precipitation amounts inferred from ASTER SMB are more than those from Pléiades or stake SMB datasets, which can be >500 mm at the terminus of Argentière Glacier (Fig. 10b) and >1000 mm at the terminus of Parlung No.4 Glacier (Fig. 7l and 7p). Performing the inference using both observed albedo and stake SMB at the on-glacier weather station on the terminus of Parlung No. 4 Glacier produces precipitation estimates of 1150 mm, up to 1300 mm less than using ASTER SMB and remotely sensed albedo (Fig. 7l), highlighting the importance of high quality geodetic observations for this methodology. By contrast, prior range and inferred meteorology are generally similar between ASTER and TanDEM-X SMB datasets on Aletsch (Fig. S4c-d and Fig. 10c-d).

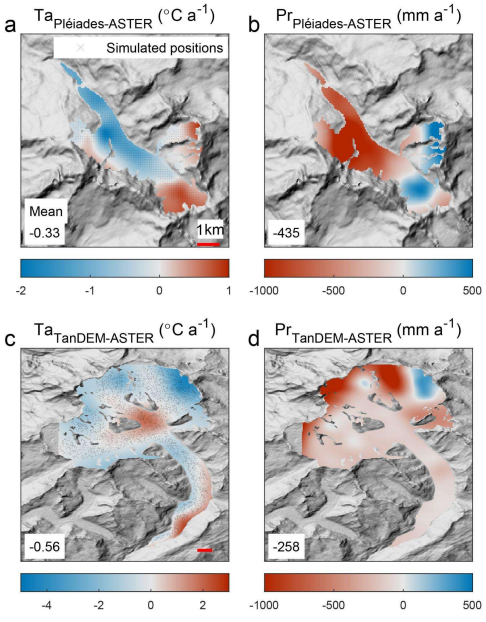

Figure 10. Difference of inferred air temperature (Ta) and precipitation (Pr) between high-quality SMB datasets (Pléiades 2013-2022/TanDEM-X 2011-2017) and ASTER SMB (2015-2019) at Argentière (a-b) and Aletsch (c-d) Glaciers. Note that the periods of meteorology are slightly different due to available SMB datasets.

Regarding the seasonal mass balance, the negative impact of ASTER SMB data quality (as above) can be partially offset by the use of satellite albedo data. By leveraging satellite albedo, the accuracy of modelled seasonal mass balance is indeed improved compared to that without albedo (Fig. 11), while there are still large errors at Parlung No.4 Glacier (Fig. 9h). The posterior distributions are mainly determined by the multitemporal albedo data when the prior, which has been defined by the SMB data, is similar (Section 4.1, Fig. 4 and S4), therefore resulting in a similar modelled seasonal mass balance between the use of Pleiades or TanDEM-X

https://doi.org/10.5194/egusphere-2026-2524
Preprint. Discussion started: 28 May 2026

versus ASTER SMB for Argentiere and Altesch glaciers, respectively. However, if the priors are strongly inappropriate, such as for the ablation region of Parlung No.4 Glacier, it is difficult to derive reliable modelled seasonal mass balances. This impact should be confirmed with additional higher-quality datasets at other sites, where possible. Interestingly, even with high-quality SMB data, substantial discrepancies (~2 m w.e.) persist in summer and annual mass balance near the glacier terminus, likely due to presence of debris (Herreid and Pellicciotti, 2020; Storni et al., 2020). We focus on largely clean-ice glaciers in this study, but treat those limited debris-covered ice areas as clean ice to avoid introducing more unknown parameters related to debris processes within T&C at this stage. However, this may lead to an modelled underestimation of mass loss in areas with thin debris cover and dirty ice (Cuffey and Paterson, 2010; Evatt et al., 2015), particularly at glacier termini with high air temperatures. Together, these comparisons highlight the crucial role of SMB in determining the prior range, as well as the potential negative influence of biased SMB modelled from the inferred meteorology.

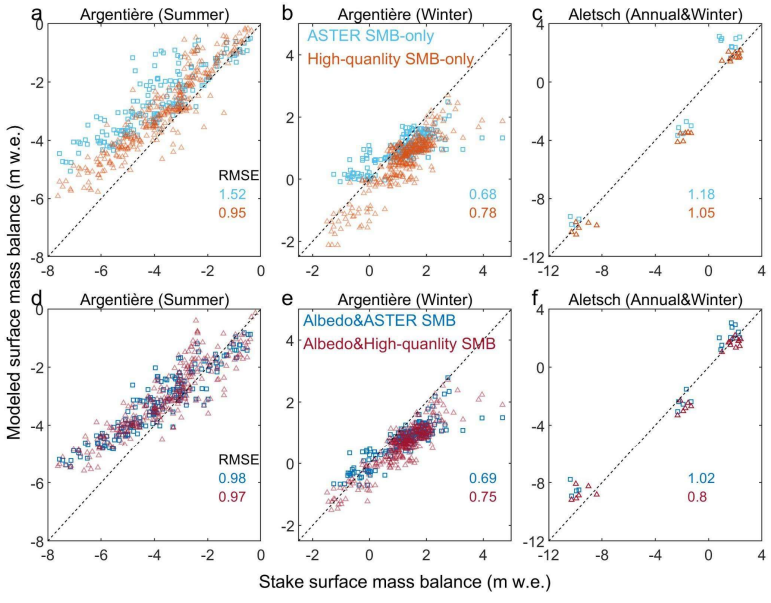

Figure 11. Annual/seasonal mass balance derived by inference framework with ASTER or high-quality SMB datasets (Pléiades 2013-2022 for Argentière Glacier and TanDEM-X 2011-2017 for Aletsch Glacier) against stake SMB on the two glaciers. Light blue and red indicate interference with SMB datasets only (a-c), dark blue and red indicate interference with both satellite albedo and SMB datasets (d-f). Each point represents an individual stake SMB measurement.

5.3 limitations of the input reanalysis data

Large overestimation of precipitation in the ablation region of Abramov Glacier is likely caused by the inaccurate representation of land surface conditions from the ERA5-Land reanalysis dataset. Specifically, the ERA5-Land land cover map is generated by a regridding of 1 km AVHRR data, therefore a misclassification of glaciers as rock/bare land/desert across much of the Pamir Alay could occur due to mixed pixels of coarse AVHRR image, especially when glacier surfaces are covered by dark debris (Fig. 12, Loveland et al., 2000). Surfaces that are erroneously classified as non-glacier experience a strong warm bias and wrong seasonality

https://doi.org/10.5194/egusphere-2026-2524
Preprint. Discussion started: 28 May 2026

due to the overestimation of sensible heat fluxes from the surface (Yang et al., 2017). We utilise a strongly negative prior [-7.6, -0.6] for air temperature correction in order to permit a better alignment of modelled mass balances with observations (Section 3.4.1), but the air temperature in the ablation region may still be overestimated, leading to very high precipitation estimates to compensate for the remaining disagreement with observations. Moreover, wrong air temperature seasonality makes it more difficult to have a successful inference. Since this misclassification only happens at a few specific regions, the impact is likely limited but highlights the importance of verifying land cover classification before inference. While we did not test our approach against alternative reanalysis or input forcing data, the expected adjustments of air temperature and precipitation (e.g. Fig. 7) may be even greater if utilising a coarser gridded data with a poorer representation of the land surface.

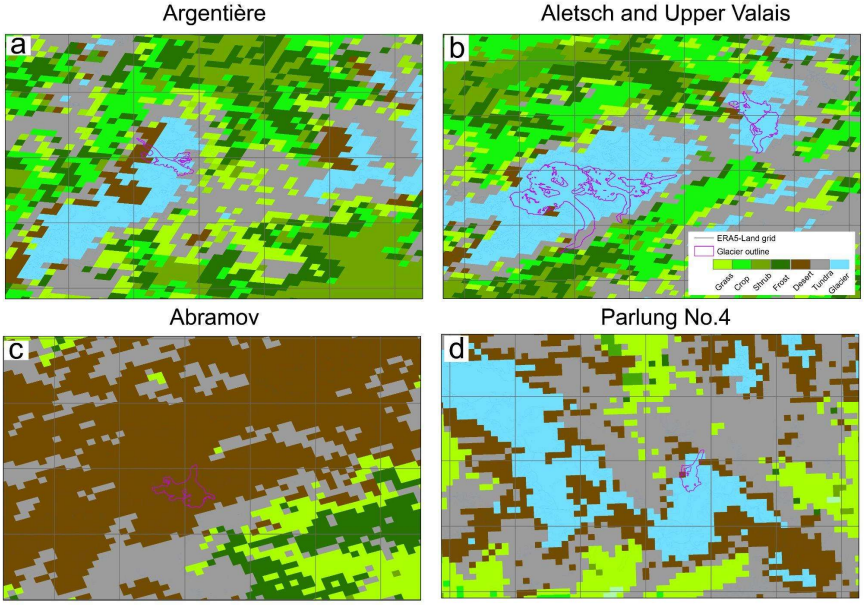

Figure 12. Land cover map (1 km) used by ERA5-Land reanalysis data. The classifications were simplified into the main types for clarity according to the original Global Land Cover Characterization (https://doi.org/10.5066/F7GB230D). a) is Argentière (FR), b) is Altesch and the Upper Valais region (CH), c) is Abramov (KZ), d) is Parlung 4 (CN). Grey outline indicates 0.1° ERA5-Land grid, purple outline indicates glacier, and colors indicate land cover type.

5.4 Reliability of inferred glacier meteorology and mass balance

Inferred air temperature and precipitation over the four study glaciers exhibit complex spatial patterns compared to the statistically downscaled reanalysis (Fig. 6, Fig. 7+S3), including mostly shallower temperature lapse rates and stronger and more variable elevation gradients of precipitation (Fig. 6, Fig. S13). This provides valuable information about the sub-pixel variability of these key meteorological variables that cannot be well resolved without dynamical downscaling, offering an alternative means of exploring high resolution meteorology over glaciers. Numerous studies have demonstrated that air temperature lapse rates over glacier surfaces are highly nonlinear due to complex heat exchanges between glaciers and their surroundings, including the effects of debris

https://doi.org/10.5194/egusphere-2026-2524
Preprint. Discussion started: 28 May 2026

cover and katabatic winds (Ayala et al., 2015; Shaw et al., 2023; Troxler et al., 2020; Yang et al., 2022). Reported lapse rates from the literature range from +5 to −12 °C km⁻¹ under different prevailing conditions, highlighting substantial variability from glacier to glacier, but also that lapse rates can often become shallower over melting glaciers. These findings are consistent with our results, which reveal pronounced elevation-dependent variability of inferred air temperatures, but with shallower lapse rates on average compared to the statistical downscaling (Fig. 7). Similarly, previous studies have documented strong, site-specific vertical precipitation gradients (e.g., Avanzi et al., 2021; Benoit et al., 2024; Buri et al., 2023; Graves et al., 2026; Immerzeel et al., 2014; Jiang et al., 2022), in agreement with the spatial variability observed across the four glaciers examined here (Fig. 6-7). Direct evaluations against on-glacier air temperature observations are necessary to quantify the accuracy of inferred meteorology, which can be addressed by applying our method in other glaciers with long-term station observations. Unfortunately, few multi-year meteorological observations exist on or directly next to glaciers in order to provide an exhaustive evaluation of the inferred meteorology (Sauter et al., 2026), especially so for robust pluviometer records, which rarely exist on the glacier surface itself. Nevertheless, inferred precipitation amounts are in close alignment with the nearby pluviometer records in the Swiss Alps (Fig. 8), lending support to the corrections and spatial coherence of precipitation achieved by the methodology.

Overall, the accuracy of the derived seasonal mass balance is comparable to that reported in previous modeling studies. RMSEs range from 0.2 to 1 m w.e. when using Bayesian inference constrained by stake mass-balance observations (Sjursen et al., 2023), and from 0.6 to 1 m w.e. in machine-learning-based approaches applied in mainland Norway and Swiss Alps (Meer et al., 2025; Sjursen et al., 2025). Consistent with our findings, Cremona et al. (2025) also report an underestimation of mass loss in regions of strong ablation in the Swiss Alps. Because their approach relies on satellite snow cover to calibrate an empirical model, seasonal biases in meteorological forcing and presence of debris at glacier terminus are not explicitly addressed, further highlighting the necessity of considering their effects in the future work.

5.5 Outlook

The key outcome of our method is the calculation of fully distributed on-glacier meteorology and seasonal mass balance over large glacier domains. By leveraging distributed satellite-derived albedo and SMB datasets, our results demonstrate that spatial corrections constrained by these observations can infer more accurate glacier meteorology and surface mass balance than a simple statistical downscaling approach (Fig. 7 and Fig. S3+9). Parameter equifinality can be substantially reduced with multitemporal albedo observations that have become widely available (Naegeli et al., 2017; Ren et al., 2024b; Xie et al., 2024), thereby improving the stability of the inferred meteorological variables and enhancing the robustness of the method when applied over large areas. This is moreover supported by initial tests conducted across multiple glaciers in the Upper Valais region of Switzerland that demonstrate that the inferred precipitation patterns are coherent among these glaciers (Fig. 8). Given the importance of the SMB data for the prior estimation (Section 5.2), careful selection of low-uncertainty ASTER SMB is essential to avoid adopting inappropriate prior ranges and potential compensatory effects of other parameters (i.e., a precipitation increase to compensate for too warm temperatures).

https://doi.org/10.5194/egusphere-2026-2524
Preprint. Discussion started: 28 May 2026

A key opportunity from this work is the derivation of glacier meteorology over long time periods. The main obstacle to achieving this goal is the availability of distributed SMB datasets: current ASTER-derived SMB products are restricted to relatively short time periods (e.g., 2015–2019) or long periods but not globally available (Miles et al., 2021). In contrast, glacier albedo datasets are available at high temporal resolution through the combination of multiple satellite sensors such as Landsat series (Wulder et al., 2019), Sentinel-2 (Ju et al., 2025), and ASTER (Abrams et al., 2002), with revisit times shorter than four days, and can potentially provide observational records exceeding 40 years. An albedo-only inference framework can in some cases derive similar spatial patterns of meteorology and mass balance compared to the albedo-SMB inference (Fig. S15), and contrary to using a SMB-only framework (Fig. S16). This highlights the dominant role of albedo in the inference procedure (Fig. 4 and S5). However, our approach still strongly relies on SMB for prior determination. Future inferences will therefore benefit from more accessible and temporally refined satellite albedo and SMB estimates.

6 Conclusions

In this study, we develop a meteorological bias correction framework to infer two key glacier meteorological variables—air temperature and precipitation—and their spatial patterns over glaciers, and seasonal glacier mass balance. We accomplish this by coupling physical modeling with globally available satellite-derived glacier surface albedo and surface mass balance datasets in a Bayesian inference framework. Our main findings are:

- Parameter equifinality can be substantially reduced by leveraging physical modeling together with quantitative and multitemporal satellite-derived albedo observations.
- A spatially variable correction of air temperature and precipitation is necessary to align the model with distributed satellite/stake observations of mass balance.
- Our framework can improve multi-year average on-glacier temperature and precipitation estimations. Compared to directly downscaled climate reanalysis data, the inferred meteorology shows improved agreement with in-situ station observations and exhibits strong spatial variability across and near glaciers, including enhanced vertical precipitation gradients and shallower above-glacier temperature lapse rates.
- Our framework offers a promising means of deriving modelled seasonal mass balances from single snapshot geodetic mass balance observations. Reconstructed annual and seasonal mass balances achieve RMSEs of <1.5 m w.e. and <1 m w.e. relative to in-situ stake measurements, which corresponds to improvements of 40-50% and 20-60%, respectively, compared to modelled mass balances without inference.

Although further evaluations are recommended, plausible magnitudes and spatial coherence of inferred catchment meteorology highlight the potential of this framework to derive spatial patterns of air temperature and precipitation from regional to global scales. The growing availability of long-term satellite albedo and surface mass balance observations further opens new opportunities for our inference framework to investigate long-term glacier changes.

Code and data availability: The source code of the land-surface model is available here:

https://doi.org/10.5194/egusphere-2026-2524
Preprint. Discussion started: 28 May 2026

https://github.com/simonefatichi/TeC_Source_Code. The point surface mass balance data were obtained from the WGMS programme (https://wgms.ch/) and ERA5-Land gridded data (hourly and monthly) were extracted from the Copernicus website: https://doi.org/10.24381/cds.68d2bb3.

Author contributions. S.R., E.M. and F.P. designed the study with T.S., M.M, and A.J., who provided regular feedback and discussion for methodology development. S.R., E.M., M.M. and M.K. collected the data, A.G. and P.G. contributed to the development of Bayesian inference, M.M, A.J. and P.B. contributed to the model simulations, SR analyzed and visualized the results. F.P. and E.M. supervised the research. S.R. wrote the initial manuscript with revisions from all authors.

Competing interests: The authors declare no competing interests.

Acknowledgements: This research received funding from the European Union's Horizon Europe research and innovation programme under the Marie Sklodowska-Curie Postdoctoral Fellowship grant agreement No. 101210216, INGEST (Inferring glacier meteorology through physical modeling and remote sensing) and Swiss Government Excellence Postdoctoral Scholarship. Marin Kneib acknowledges funding from the Swiss National Science Foundation (SNSF) under the 'Contribution of avalanches to glacier mass balance at the global scale' (CAIRN-GLOBAL) Postdoc Mobility program (grant agreement P5R5PN_225605). We would like to acknowledge the use of the Google Earth Engine platform for glacier albedo processing. We also thank the European Space Agency (ESA) for the Copernicus Sentinel-2 data and the U.S. Geological Survey (USGS) for providing the Landsat imagery used in this research.

References

Aberle, R., Enderlin, E. M., Rounce, D. R., O'Neel, S., Tober, B., and Friel, A.: Leveraging weekly snow cover time series for improved glacier monitoring and modeling, Geophys. Res. Lett., 52, 2025 115523, 2025.

Abrams, M., Hook, S., and Ramachandran, B.: ASTER user handbook, version 2, Jet Propuls. Lab., 4800, 135, 2002.

Aguayo, R., Zekollari, H., Hanus, S., Baez-Villanueva, O. M., Mendoza, P. A., and Maussion, F.: Hybrid Glacio-Hydrological Modeling Reveals Contrasting Runoff Changes in Western Patagonia Over the 21st Century, Earths Future, 13, e2025EF006442, https://doi.org/10.1029/2025EF006442, 2025.

Arduini, G., Rüdiger, C., and Balsamo, G.: Enhancing the Representation of Glaciers and Ice Sheets in the ecLand Land-Surface Model: Impacts on Surface Energy Balance and Hydrology Across Scales, The Cryosphere, 20, 1119–1137, 2026.

Arndt, A. and Schneider, C.: Spatial pattern of glacier mass balance sensitivity to atmospheric forcing in High Mountain Asia, J. Glaciol., 69, 1616–1633, https://doi.org/10.1017/jog.2023.46, 2023.

Avanzi, F., Ercolani, G., Gabellani, S., Cremonese, E., Pogliotti, P., Filippa, G., Cella, U., Ratto, S., Stevenin, H., Cauduro, M., and Juglair, S.: Learning about precipitation lapse rates from snow course data improves water balance modeling, Hydrol. Earth Syst. Sci., 25, 2109–2131, 2021.

Ayala, A., Pellicciotti, F., and Shea, J. M.: Modeling 2 m air temperatures over mountain glaciers: Exploring the influence of katabatic cooling and external warming, J. Geophys. Res. Atmospheres, 120, 3139–3157,

https://doi.org/10.5194/egusphere-2026-2524
Preprint. Discussion started: 28 May 2026

2015.

Barandun, M. and Pohl, E.: Central Asia's spatiotemporal glacier response ambiguity due to data inconsistencies and regional simplifications, The Cryosphere, 17, 1343–1371, 2023.

Benoit, L., Koch, E., Peleg, N., and Mariethoz, G.: Precipitation-elevation relationship: Non-linearity and space–time variability prevail in the Swiss Alps, J. Hydrol. X, 25, 100186, 2024.

Bolibar, J., Rabatel, A., Gouttevin, I., Zekollari, H., and Galiez, C.: Nonlinear sensitivity of glacier mass balance to future climate change unveiled by deep learning, Nat. Commun., 13, 1–11, https://doi.org/10.1038/s41467-022-28033-0, 2022.

Buri, P., Fatichi, S., Shaw, T. E., Miles, E. S., McCarthy, M. J., Fyffe, C. L., Fugger, S., Ren, S., Kneib, M., Jouberton, A., Steiner, J., Fujita, K., and Pellicciotti, F.: Land Surface Modeling in the Himalayas: On the Importance of Evaporative Fluxes for the Water Balance of a High-Elevation Catchment, Water Resour. Res., 59, https://doi.org/10.1029/2022WR033841, 2023.

Cannon, A. J.: Multivariate quantile mapping bias correction: an N-dimensional probability density function transform for climate model simulations of multiple variables, Clim. Dyn., 50, 31–49, 2018.

Collier, E., Ban, N., Richter, N., Ahrens, B., Chen, D., Chen, X., and Lai, H.-W.: The first ensemble of kilometer-scale simulations of a hydrological year over the third pole, Clim. Dyn., 62, 7501–7518, 2024.

Cook, M., Schott, J. R., Mandel, J., and Raqueno, N.: Development of an operational calibration methodology for the Landsat thermal data archive and initial testing of the atmospheric compensation component of a land surface temperature (LST) product from the archive, Remote Sens., 6, 11244–11266, https://doi.org/10.3390/rs61111244, 2014.

Cosgrove, B. A., Lohmann, D., Mitchell, K. E., Houser, P. R., Wood, E. F., Schaake, J. C., and Meng, J.: Real-time and retrospective forcing in the North American Land Data Assimilation System (NLDAS) project, J. Geophys. Res. Atmospheres, 108, 2003.

Cremona, A., Huss, M., Landmann, J. M., Schwaizer, G., Paul, F., and Farinotti, D.: Constraining sub-seasonal glacier mass balance in the Swiss Alps using Sentinel-2-derived snow-cover observations, J. Glaciol., 71, 25, 2025.

Cuffey, K. M. and Paterson, W. S. B.: The physics of glaciers, Academic Press, 2010.

Ding, B., Yang, K., Qin, J., Wang, L., Chen, Y., and He, X.: The dependence of precipitation types on surface elevation and meteorological conditions and its parameterization, J. Hydrol., 513, 154–163, https://doi.org/10.1016/j.jhydrol.2014.03.038, 2014.

Ding, B., Yang, K., Yang, W., He, X., Chen, Y., Lazhu, Guo, X., Wang, L., Wu, H., and Yao, T.: Development of a Water and Enthalpy Budget-based Glacier mass balance Model (WEB-GM) and its preliminary validation, Water Resour. Res., 53, 3146–3178, https://doi.org/10.1002/2016WR018865, 2017.

Draeger, C., Radić, V., White, R. H., and Tessema, M. A.: Evaluation of reanalysis data and dynamical downscaling for surface energy balance modeling at mountain glaciers in western Canada, The Cryosphere, 18, 17–42, https://doi.org/10.5194/tc-18-17-2024, 2024.

Evatt, G. W., Abrahams, I. D., Heil, M., Mayer, C., Kingslake, J., Mitchell, S. L., Fowler, A. C., and Clark, C. D.: Glacial melt under a porous debris layer, J. Glaciol., 61, 825–836, 2015.

Fatichi, S., Ivanov, V. Y., and Caporali, E.: A mechanistic ecohydrological model to investigate complex interactions in cold and warm water-controlled environments : 1 . Theoretical framework and plot-scale

https://doi.org/10.5194/egusphere-2026-2524
Preprint. Discussion started: 28 May 2026

analysis, 4, 1–31, https://doi.org/10.1029/2011MS000086, 2012a.

Fatichi, S., Ivanov, V. Y., and Caporali, E.: A mechanistic ecohydrological model to investigate complex interactions in cold and warm water-controlled environments: 1. Theoretical framework and plot-scale analysis, J. Adv. Model. Earth Syst., 4, 1–31, https://doi.org/10.1029/2011MS000086, 2012b.

Fontrodona-Bach, A., Groeneveld, L., Miles, E., McCarthy, M., Shaw, T., Melo Velasco, V., and Pellicciotti, F.: DebDaB: a database of supraglacial debris thickness and physical properties, Earth Syst. Sci. Data, 17, 4213–4234, https://doi.org/10.5194/essd-17-4213-2025, 2025.

Fugger, S., Fyffe, C. L., Fatichi, S., Miles, E., McCarthy, M., Shaw, T. E., and Ding, B.: Understanding monsoon controls on the energy and mass balance of glaciers in the Central and Eastern Himalaya, The Cryosphere, 16, 1631–1652, 2022.

Fugger, S., Shaw, T. E., Jouberton, A., Miles, E. S., Buri, P., McCarthy, M., Fyffe, C., Fatichi, S., Kneib, M., Molnar, P., and Pellicciotti, F.: Hydrological regimes and evaporative flux partitioning at the climatic ends of high mountain Asia, Environ. Res. Lett., 19, 044057, https://doi.org/10.1088/1748-9326/ad25a0, 2024.

Fyffe, C. L., Potter, E., Fugger, S., Orr, A., Fatichi, S., Loarte, E., and Medina, K.: The energy and mass balance of Peruvian glaciers, J. Geophys. Res. Atmospheres, 126, 2021 034911, 2021.

Gabbi, J., Carenzo, M., Pellicciotti, F., Bauder, A., and Funk, M.: A comparison of empirical and physically based glacier surface melt models for long-term simulations of glacier response, J. Glaciol., 60, 1140–1154, 2014.

Girona-Mata, M., Orr, A., Widmann, M., Bannister, D., Dars, G. H., Hosking, S., and Norris, J.: Probabilistic precipitation downscaling for ungauged mountain sites: a pilot study for the Hindu Kush Karakoram Himalaya, EGUsphere, 1–33, 2024.

Graves, B., Matthews, T., Perry, L. B., Edwards, T., Taylor, R., Brun, F., Wagnon, P., Khadka, A., and Shrestha, D.: Modelling accumulation of a high-altitude Himalayan glacier, J. Glaciol., 72, e32, https://doi.org/10.1017/jog.2026.10147, 2026.

Haeberli, W., Hoelzle, M., Paul, F., and Zemp, M.: Integrated monitoring of mountain glaciers as key indicators of global climate change: the European Alps, Ann. Glaciol., 46, 150–160, 2007.

Herreid, S. and Pellicciotti, F.: The state of rock debris covering Earth's glaciers, Nat. Geosci., 13, 621–627, https://doi.org/10.1038/s41561-020-0615-0, 2020.

Hock, R.: Glacier melt: a review of processes and their modelling, Prog. Phys. Geogr., 29, 362–391, 2005.

Hugonnet, R., McNabb, R., Berthier, E., Menounos, B., Nuth, C., Girod, L., Farinotti, D., Huss, M., Dussaillant, I., Brun, F., and Kääb, A.: Accelerated global glacier mass loss in the early twenty-first century, Nature, 592, 726–731, https://doi.org/10.1038/s41586-021-03436-z, 2021.

Immerzeel, W. W., Petersen, L., Ragettli, S., and Pellicciotti, F.: The importance of observed gradients of air temperature and precipitation for modeling runoff from a glacierized watershed in the Nepalese Himalayas, Water Resour. Res., 50, 2212–2226, 2014.

Immerzeel, W. W., Wanders, N., Lutz, A. F., Shea, J. M., and Bierkens, M. F. P.: Reconciling high-altitude precipitation in the upper Indus basin with glacier mass balances and runoff, Hydrol. Earth Syst. Sci., 19, 4673–4687, https://doi.org/10.5194/hess-19-4673-2015, 2015.

Isotta, F. A., Frei, C., Weilguni, V., Perčec Tadić, M., Lassègues, P., Rudolf, B., Pavan, V., Cacciamani, C., Antolini, G., Ratto, S. M., Munari, M., Micheletti, S., Bonati, V., Lussana, C., Ronchi, C., Panettieri, E.,

https://doi.org/10.5194/egusphere-2026-2524
Preprint. Discussion started: 28 May 2026

Marigo, G., and Vertačnik, G.: The climate of daily precipitation in the Alps: development and analysis of a high-resolution grid dataset from pan-Alpine rain-gauge data, Int. J. Climatol., 34, 1657–1675, https://doi.org/10.1002/joc.3794, 2014.

Jiang, Y., Yang, K., Yang, H., Lu, H., Chen, Y., Zhou, X., Sun, J., Yang, Y., and Wang, Y.: Characterizing basin-scale precipitation gradients in the Third Pole region using a high-resolution atmospheric simulation-based dataset, Hydrol. Earth Syst. Sci., 26, 4587–4601, 2022.

Johnson, E. and Rupper, S.: An Examination of Physical Processes That Trigger the Albedo-Feedback on Glacier Surfaces and Implications for Regional Glacier Mass Balance Across High Mountain Asia, Front. Earth Sci., 8, 1–18, https://doi.org/10.3389/feart.2020.00129, 2020.

Jouberton, A., Shaw, T. E., Miles, E., McCarthy, M., Fugger, S., Ren, S., Dehecq, A., Yang, W., and Pellicciotti, F.: Warming-induced monsoon precipitation phase change intensifies glacier mass loss in the southeastern Tibetan Plateau, Proc. Natl. Acad. Sci. U. S. A., 119, 1–7, https://doi.org/10.1073/pnas.2109796119, 2022.

Jouberton, A., Shaw, T. E., Miles, E., Kneib, M., Fugger, S., Buri, P., McCarthy, M., Kayumov, A., Navruzshoev, H., and Halimov, A.: Snowfall decrease in recent years undermines glacier health and meltwater resources in the Northwestern Pamirs, Commun. Earth Environ., 6, 691, 2025.

Ju, J., Zhou, Q., Freitag, B., Roy, D. P., Zhang, H. K., Sridhar, M., Mandel, J., Arab, S., Schmidt, G., Crawford, C. J., Gascon, F., Strobl, P. A., Masek, J. G., and Neigh, C. S. R.: The Harmonized Landsat and Sentinel-2 version 2.0 surface reflectance dataset, Remote Sens. Environ., 324, 114723, https://doi.org/10.1016/j.rse.2025.114723, 2025.

Khadka, A., Wagnon, P., Brun, F., Shrestha, D., Lejeune, Y., and Arnaud, Y.: Evaluation of ERA5-Land and HARv2 reanalysis data at high elevation in the upper Dudh Koshi basin (Everest region, Nepal, J. Appl. Meteorol. Climatol., 61, 931–954, 2022.

Khadka, A., Brun, F., Wagnon, P., Shrestha, D., and Sherpa, T. C.: Surface energy and mass balance of Mera Glacier (Nepal, Central Himalaya) and their sensitivity to temperature and precipitation, J. Glaciol., 1–22, 2024.

Kneib, M., Dehecq, A., Gilbert, A., Basset, A., Miles, E. S., Jouvet, G., and Jourdain, B.: Distributed surface mass balance of an avalanche-fed glacier, The Cryosphere, 18, 5965–5983, 2024.

Leinss, S. and Bernhard, P.: TanDEM-X: Deriving InSAR height changes and velocity dynamics of great aletsch glacier, IEEE J. Sel. Top. Appl. Earth Obs. Remote Sens., 14, 4798–4815, 2021.

Liston, G. E. and Elder, K.: A meteorological distribution system for high-resolution terrestrial modeling (MicroMet, J. Hydrometeorol., 7, 217–234, 2006.

Liu, J. S.: Monte Carlo Strategies in Scientific Computing, Springer New York, New York, NY, https://doi.org/10.1007/978-0-387-76371-2, 2004.

Loveland, T. R., Reed, B. C., Brown, J. F., Ohlen, D. O., Zhu, Z., Yang, L., and Merchant, J. W.: Development of a global land cover characteristics database and IGBP DISCover from 1 km AVHRR data, Int. J. Remote Sens., 21, 1303–1330, https://doi.org/10.1080/014311600210191, 2000.

Machguth, H., Paul, F., Kotlarski, S., and Hoelzle, M.: Calculating distributed glacier mass balance for the Swiss Alps from regional climate model output: A methodical description and interpretation of the results, J. Geophys. Res. Atmospheres, 114, 2009.

Mackintosh, A. N., Anderson, B. M., Lorrey, A. M., Renwick, J. A., Frei, P., and Dean, S. M.: Regional cooling

https://doi.org/10.5194/egusphere-2026-2524
Preprint. Discussion started: 28 May 2026

caused recent New Zealand glacier advances in a period of global warming, Nat. Commun., 8, 14202, https://doi.org/10.1038/ncomms14202, 2017.

Marzeion, B., Hock, R., Anderson, B., Bliss, A., Champollion, N., Fujita, K., Huss, M., Immerzeel, W. W., Kraaijenbrink, P., Malles, J. H., Maussion, F., Radić, V., Rounce, D. R., Sakai, A., Shannon, S., van de Wal, R., and Zekollari, H.: Partitioning the Uncertainty of Ensemble Projections of Global Glacier Mass Change, Earths Future, 8, https://doi.org/10.1029/2019EF001470, 2020.

McCarthy, M.: A MATLAB toolbox for statistical downscaling of climate reanalysis data (Version 1.0.0). GitHub, 2025.

McCarthy, M., Meier, F., Fatichi, S., Stocker, B. D., Shaw, T. E., Miles, E., and Pellicciotti, F.: Glacier contributions to river discharge during the current Chilean megadrought, Earths Future, 10, 2022 002852, 2022.

Meer, Marijn, H. Z., Huss, M., Bolibar, J., Sjursen, K. H., and Farinotti, D.: A minimal machine-learning glacier mass balance model, The Cryosphere, 19, 805–826, 2025.

Melo-Velasco, V., Miles, E., McCarthy, M., Shaw, T. E., Fyffe, C., Fontrodona-Bach, A., and Pellicciotti, F.: Method Dependence in Thermal Conductivity and Aerodynamic Roughness Length Estimates on a Debris-Covered Glacier, J. Geophys. Res. Earth Surf., 130, e2025JF008360, https://doi.org/10.1029/2025JF008360, 2025.

Miao, C., Hu, J., Moradkhani, H., and Destouni, G.: Hydrological Research Evolution: A Large Language Model-Based Analysis of 310,000 Studies Published Globally Between 1980 and 2023, Water Resour. Res., 60, e2024WR038077, https://doi.org/10.1029/2024WR038077, 2024.

Miles, E., McCarthy, M., Dehecq, A., Kneib, M., Fugger, S., and Pellicciotti, F.: Health and sustainability of glaciers in High Mountain Asia, Nat. Commun., 12, 2868–2877, https://doi.org/10.1038/s41467-021-23073-4, 2021.

Miles, E. S., Steiner, J. F., Buri, P., Immerzeel, W. W., and Pellicciotti, F.: Controls on the relative melt rates of debris-covered glacier surfaces, Environ. Res. Lett., 17, 064004, https://doi.org/10.1088/1748-9326/ac6966, 2022.

Millan, R., Mouginot, J., Rabatel, A., and Morlighem, M.: Ice velocity and thickness of the world's glaciers, Nat. Geosci., 15, 124–129, https://doi.org/10.1038/s41561-021-00885-z, 2022.

Muñoz-Sabater, J., Dutra, E., Agustí-Panareda, A., Albergel, C., Arduini, G., Balsamo, G., and Boussetta, S.: ERA5-Land: A state-of-the-art global reanalysis dataset for land applications, Earth Syst. Sci. Data, 13, 4349–4383, 2021.

Naegeli, K., Damm, A., Huss, M., Wulf, H., Schaepman, M., and Hoelzle, M.: Cross-comparison of albedo products for glacier surfaces derived from airborne and satellite (Sentinel-2 and Landsat 8) optical data, Remote Sens., 9, 110, 2017.

Oberrauch, M., Cluzet, B., Magnusson, J., and Jonas, T.: Improving Fully Distributed Snowpack Simulations by Mapping Perturbations of Meteorological Forcings Inferred From Particle Filter Assimilation of Snow Monitoring Data, Water Resour. Res., 60, e2023WR036994, https://doi.org/10.1029/2023WR036994, 2024.

Oerlemans, J., Anderson, B., Hubbard, A., Huybrechts, P., Johannesson, T., Knap, W. H., Schmeits, M., Stroeven, A. P., Van de Wal, R. S. W., and Wallinga, J.: Modelling the response of glaciers to climate

https://doi.org/10.5194/egusphere-2026-2524
Preprint. Discussion started: 28 May 2026

warming, Clim. Dyn., 14, 267–274, 1998.

Pepin, N. C., Arnone, E., Gobiet, A., Haslinger, K., Kotlarski, S., Notarnicola, C., Palazzi, E., Seibert, P., Serafin, S., Schöner, W., Terzago, S., Thornton, J. M., Vuille, M., and Adler, C.: Climate Changes and Their Elevational Patterns in the Mountains of the World, Rev. Geophys., 60, e2020RG000730, https://doi.org/10.1029/2020RG000730, 2022.

Ren, S., Miles, E. S., Jia, L., Menenti, M., Kneib, M., Buri, P., McCarthy, M. J., Shaw, T. E., Yang, W., and Pellicciotti, F.: Anisotropy parameterization development and evaluation for glacier surface albedo retrieval from satellite observations, Remote Sens., 13, https://doi.org/10.3390/rs13091714, 2021.

Ren, S., Yao, T., Yang, W., Miles, E. S., Zhao, H., and Zhu, M.: Changes in glacier surface temperature across the Third Pole from 2000 to 2021, Remote Sens. Environ., 305, 114076, https://doi.org/10.1016/j.rse.2024.114076, 2024a.

Ren, S., Jia, L., Miles, E. S., Menenti, M., Kneib, M., Shaw, T. E., Buri, P., McCarthy, M. J., Yang, W., Pellicciotti, F., and Yao, T.: Observed and projected declines in glacier albedo across the Third Pole in the 21st century, One Earth, 7, 1587–1599, https://doi.org/10.1016/j.oneear.2024.08.010, 2024b.

Réveillet, M., Six, D., Vincent, C., Rabatel, A., Dumont, M., Lafaysse, M., Morin, S., Vionnet, V., and Litt, M.: Relative performance of empirical and physical models in assessing the seasonal and annual glacier surface mass balance of Saint-Sorlin Glacier (French Alps, The Cryosphere, 12, 1367–1386, 2018.

Richter, J. N., Arndt, A., Ban, N., Gampierakis, N., Maussion, F., Prinz, R., Scheiter, M., Umlauf, N., and Nicholson, L.: Towards the Bayesian calibration of a glacier surface energy balance model for unmonitored glaciers, EGUsphere, 2026, 1–47, 2026.

Rouf, T., Mei, Y., Maggioni, V., Houser, P., and Noonan, M.: A physically based atmospheric variables downscaling technique, J. Hydrometeorol., 21, 93–108, 2020.

Rounce, D. R., Khurana, T., Short, M. B., Hock, R., Shean, D. E., and Brinkerhoff, D. J.: Quantifying parameter uncertainty in a large-scale glacier evolution model using Bayesian inference: application to High Mountain Asia, J. Glaciol., 66, 175–187, 2020.

Rounce, D. R., Hock, R., McNabb, R. W., Millan, R., Sommer, C., Braun, M. H., Malz, P., Maussion, F., Mouginot, J., Seehaus, T. C., and Shean, D. E.: Distributed Global Debris Thickness Estimates Reveal Debris Significantly Impacts Glacier Mass Balance, Geophys. Res. Lett., 48, e2020GL091311, https://doi.org/10.1029/2020GL091311, 2021.

Rounce, D. R., Hock, R., Maussion, F., Hugonnet, R., Kochtitzky, W., Huss, M., Berthier, E., Brinkerhoff, D., Compagno, L., Copland, L., Farinotti, D., Menounos, B., and McNabb, R. W.: Global glacier change in the 21st century: Every increase in temperature matters, Science, 379, 78–83, https://doi.org/10.1126/science.abo1324, 2023.

Rye, C. J., Arnold, N. S., Willis, I. C., and Kohler, J.: Modeling the surface mass balance of a high Arctic glacier using the ERA-40 reanalysis, J. Geophys. Res. Earth Surf., 115, 2010.

Salerno, F., Guyennon, N., Yang, K., Shaw, T. E., Lin, C., Romano, E., Gruber, S., Bolch, T., Alessandri, A., Putero, D., Diolaiuti, G., Tartari, G., Verza, G., Balsamo, G., Miles, E. S., and Pellicciotti, F.: Local cooling and drying induced by Himalayan glaciers under global warming, Nat. Geosci., 16, 1120–1127, https://doi.org/10.1038/s41561-023-01331-y, 2023.

Sauter, T., Brock, B. W., Collier, E., Goger, B., Groos, A. R., Haualand, K. F., Mott, R., Nicholson, L., Prinz,

https://doi.org/10.5194/egusphere-2026-2524
Preprint. Discussion started: 28 May 2026

R., Shaw, T. E., Stiperski, I., Georgi, A., Haugeneder, M., Mandal, A., Reynolds, D., Saigger, M., Sicart, J. E., and Voordendag, A.: Glacier-Atmosphere Interactions and Feedbacks in High-Mountain Regions - A Review, Rev. Geophys., 64, e2024RG000869, https://doi.org/10.1029/2024RG000869, 2026.

Schuster, L., Maussion, F., Rounce, D., Ultee, L., Schmitt, P., Lacroix, F., Frölicher, T., and Schleussner, C.-F.: Irreversible glacier change and trough water for centuries after overshooting 1.5° C, 2024.

Shaw, T. E., Yang, W., Ayala, Á., Bravo, C., Zhao, C., and Pellicciotti, F.: Distributed summer air temperatures across mountain glaciers in the south-east Tibetan Plateau: Temperature sensitivity and comparison with existing glacier datasets, Cryosphere, 15, 595–614, https://doi.org/10.5194/tc-15-595-2021, 2021.

Shaw, T. E., Miles, E. S., Chen, D., Jouberton, A., Kneib, M., Fugger, S., and Ou, T.: Multi-decadal monsoon characteristics and glacier response in High Mountain Asia, Environ. Res. Lett., 17, 104001, 2022.

Shaw, T. E., Buri, P., McCarthy, M., Miles, E. S., Ayala, Á., and Pellicciotti, F.: The Decaying Near-Surface Boundary Layer of a Retreating Alpine Glacier, Geophys. Res. Lett., 50, 2023 103043, 2023.

Shaw, T. E., Buri, P., McCarthy, M., Miles, E. S., and Pellicciotti, F.: Local Controls on Near-Surface Glacier Cooling Under Warm Atmospheric Conditions, J. Geophys. Res. Atmospheres, 129, e2023JD040214, https://doi.org/10.1029/2023JD040214, 2024.

Shaw, T. E., Miles, E. S., McCarthy, M., Buri, P., Guyennon, N., Salerno, F., Carturan, L., Brock, B., and Pellicciotti, F.: Mountain glaciers recouple to atmospheric warming over the twenty-first century, Nat. Clim. Change, 15, 1212–1218, 2025.

Sjursen, K. H., Dunse, T., Tambue, A., Schuler, T. V., and Andreassen, L. M.: Bayesian parameter estimation in glacier mass-balance modelling using observations with distinct temporal resolutions and uncertainties, J. Glaciol., 69, 1803–1822, 2023.

Sjursen, K. H., Bolibar, J., Meer, M., Andreassen, L. M., Biesheuvel, J. P., Dunse, T., Huss, M., Maussion, F., Rounce, D. R., and Tober, B.: Machine learning improves seasonal mass balance prediction for unmonitored glaciers, The Cryosphere, 19, 5801–5826, 2025.

Storni, E., Hugentobler, M., Manconi, A., and Loew, S.: Monitoring and analysis of active rockslide-glacier interactions (Moosfluh, Switzerland, Geomorphology, 371, 107414, 2020.

Thornton, J. M., Pepin, N., Shahgedanova, M., and Adler, C.: Coverage of in situ climatological observations in the world's mountains, Front. Clim., 4, 814181, 2022.

Torre, D., Daniele, N. D. M., Menapace, A., Avesani, D., Righetti, M., and Majone, B.: Suitability of ERA5-Land reanalysis dataset for hydrological modelling in the Alpine region, J. Hydrol. Reg. Stud., 52, 101718, 2024.

Troxler, P., Ayala, Á., Shaw, T. E., Nolan, M., Brock, B. W., and Pellicciotti, F.: Modelling spatial patterns of near-surface air temperature over a decade of melt seasons on McCall Glacier, Alaska, J. Glaciol., 66, 386–400, 2020.

Ultee, L., Wimberly, F., Coats, S., Mackay, J., and Holmgren, E.: CMIP6 climate model spread outweighs glacier model spread in 21st-century drought buffering projections, The Cryosphere, 20, 1339–1361, 2026.

Valéry, A., Andréassian, V., and Perrin, C.: Regionalization of precipitation and air temperature over high-altitude catchments–learning from outliers, Hydrol. Sci. Journal–Journal Sci. Hydrol., 55, 928–940, 2010.

Verjans, V., Leeson, A. A., Christopher Nemeth, C. M. S., Munneke, P. K., Noël, B., and Wessem, J. M.: Bayesian calibration of firn densification models, The Cryosphere, 14, 3017–3032, 2020.

https://doi.org/10.5194/egusphere-2026-2524
Preprint. Discussion started: 28 May 2026

Vogel, E., Johnson, F., Marshall, L., Bende-Michl, U., Wilson, L., Peter, J. R., and Wasko, C.: An evaluation framework for downscaling and bias correction in climate change impact studies, J. Hydrol., 622, 129693, 2023.

Williamson, S. N., Marshall, S. J., and Menounos, B.: Temperature mediated albedo decline portends acceleration of North American glacier mass loss, Commun. Earth Environ., 6, 555, 2025.

Wu, X., Su, J., Ren, W., Lü, H., and Yuan, F.: Statistical comparison and hydrological utility evaluation of ERA5-Land and IMERG precipitation products on the Tibetan Plateau, J. Hydrol., 620, 129384, 2023.

Wulder, M. A., Loveland, T. R., Roy, D. P., Crawford, C. J., Masek, J. G., Woodcock, C. E., Allen, R. G., Anderson, M. C., Belward, A. S., Cohen, W. B., Dwyer, J., Erb, A., Gao, F., Griffiths, P., Helder, D., Hermosilla, T., Hipple, J. D., Hostert, P., Hughes, M. J., Huntington, J., Johnson, D. M., Kennedy, R., Kilic, A., Li, Z., Lymburner, L., McCorkel, J., Pahlevan, N., Scambos, T. A., Schaaf, C., Schott, J. R., Sheng, Y., Storey, J., Vermote, E., Vogelmann, J., White, J. C., Wynne, R. H., and Zhu, Z.: Current status of Landsat program, science, and applications, Remote Sens. Environ., 225, 127–147, https://doi.org/10.1016/j.rse.2019.02.015, 2019.

Xie, F., Liu, S., Zhu, Y., Qing, X., Tan, S., Gao, Y., Qi, M., Yi, Y., Ye, H., Afzal, M. M., Zhang, X., and Zhou, J.: Retrieval of high-resolution melting-season albedo and its implications for the Karakoram Anomaly, Remote Sens. Environ., 315, 114438, https://doi.org/10.1016/j.rse.2024.114438, 2024.

Yang, W., Yao, T., Zhu, M., and Wang, Y.: Comparison of the meteorology and surface energy fluxes of debris-free and debris-covered glaciers in the southeastern Tibetan Plateau, J. Glaciol., 63, 1090–1104, https://doi.org/10.1017/jog.2017.77, 2017.

Yang, W., Zhu, M., Guo, X., and Zhao, H.: Air Temperature Variability in High-Elevation Glacierized Regions: Observations from Six Catchments on the Tibetan Plateau, J. Appl. Meteorol. Climatol., 61, 224–239, https://doi.org/10.1175/JAMC-D-21-0122.1, 2022.

Zekollari, H., Huss, M., Schuster, L., Maussion, F., Rounce, D. R., Aguayo, R., and Champollion, N.: Twenty-first century global glacier evolution under CMIP6 scenarios and the role of glacier-specific observations, The Cryosphere, 18, 5045–5066, 2024.

Zolles, T., Maussion, F., Galos, S. P., Gurgiser, W., and Nicholson, L.: Robust uncertainty assessment of the spatio-temporal transferability of glacier mass and energy balance models, The Cryosphere, 13, 469–489, 2019.

Zupanc, A.: Improving cloud detection with machine learning, Accessed Oct, 10, 2019, 2017.